New Research Proposal to Jefferson Lab PAC 28

Semi-Inclusive Pion Production with a Longitudinally Polarized Target at 6 GeV

H. Avakian[1,2], P. Bosted[1], S. Boyarinov, V.D. Burkert, V. Dharmawardane, L. Elouadrhiri, R. Niyazov, Yu. Sharabian, E. Smith
Jefferson Lab, Newport News, VA 23606, USA

K. Griffioen[1]
College of William & Mary, 23187, USA

D. Crabb[1], L.C. Smith
UVA, Charlottesville, VA 22904,USA

J. Ball, R. De Masi, M. Garçon, F.-X. Girod, C. Muñoz Camacho, F. Sabatié
DAPNIA/SPhN, CEA-Saclay, F-91191 Gif-sur-Yvette, France

S. Bouchigny, M. Guidal, M. Mac Cormick, H.-S. Jo and S. Niccolai
Institut de Physique Nucléaire, F-91406 Orsay, France

O. Pogorelko, S. Kuleshov, I. Bedlinsky
Institute of Theoretical and Experimental Physics, Moscow, 117259, Russia

Y. Prok
Massachusetts Institute of Technology 77 Massachusetts Avenue Cambridge, MA 02139

A. Biselli
Fairfield University, Fairfield CT 06824, USA

M. Amarian, S. Bueltmann, H. Juengst, S.E. Kuhn
Old Dominion University, Norfolk, VA 23529, USA

K. Joo, M. Ungaro
UCON, CO 23529, USA

S. Chen
Florida State University, Tallahassee, FL 32306, USA

G. Fedotov, B. Ishkhanov, E. Isupov,V. Mokeev, N. Shvedunov
119899 Vorob'evy gory, Skobeltsyn Nuclear Physics Institute at MSU,Moscow, Russia

M. Anselmino, A. Kotzinian, A. Prokhudin
Università di Torino and INFN, Sezione di Torino, Via P. Giuria 1, I-10125 Torino

F. Yuan
RBRC, Brookhaven National Laboratory, Upton, NY 11973, USA

P. Schweitzer
Ruhr-Universitat Bochum, 44780, Bochum Germany

[1]Co-spokesperson
[2]Contact person

Abstract

We propose to study single-spin and double-spin azimuthal asymmetries in semi-inclusive electroproduction of pions using the CEBAF 6 GeV polarized electron beam and the CLAS detector with a longitudinally polarized proton target and the new Inner Calorimeter.

The measurement of the $\sin 2\phi$ azimuthal moment of the target spin-dependent part of the cross section, in particular, will probe the Collins fragmentation function and provide information on the orbital momentum of quarks by measuring the leading twist transverse momentum dependent (TMD) parton distribution related to the interference between $L = 0$ and $L = 1$ light-cone wave functions.

The $\sin\phi$ moment will also be analyzed, further probing the polarization-dependence of quark hadronization as embodied in the Collins function, and allowing the study of the higher twist distribution function h_L. The z-dependence of the $\sin\phi$ and $\sin 2\phi$ asymmetries will be studied to verify the Collins mechanism for fragmentation of transversely polarized quarks, and the Q^2 dependence of the ratio of $\sin\phi$ to $\sin 2\phi$ moments will be studied to verify the hypothesis that the former is twist-3, and the later twist-2. High statistics measurements of the double spin asymmetries in inclusive and semi-inclusive pion production will be used to study the $(Q^2, W, x, P_\perp, z)$ phase space, where factorization of PDFs and fragmentation functions holds, and as a bonus provide improved knowledge of the polarized quark distribution functions. Two-pion production will also be studied to help understand the diffractive ρ^0 and other 2-pion contributions to semi-inclusive DIS.

A total of sixty days is requested: fifty days of production running, and ten days for target changes and background and calibration measurements. The experiment uses the standard CLAS configuration with the Eg1 NH_3 polarized target and the DVCS Inner Calorimeter.

Contents

1 Introduction

Orbital momentum of partons has been of central interest since the EMC [1] measurements implied that the helicity of the constituent quarks account for only a fraction of the nucleon spin. Very little is known about quark-quark correlations, the quark distribution in transverse momentum and space, and contributions of correlated quark-antiquark pairs (mesons) to the nucleon wave function.

In recent years parton distribution functions have been generalized to contain information not only on the longitudinal but also on the transverse distributions of partons in a fast moving hadron. Two major sets of non-perturbative generalized parton distributions were introduced: the Generalized Parton Distributions (GPDs) [2, 3, 4] and Transverse Momentum Dependent (TMD) parton distributions. Eight independent TMD parton distributions have been identified [5, 6, 7, 8] at leading twist, all of which are accessible in Semi-Inclusive DIS (SIDIS). Furthermore, the phase-space Wigner distributions were introduced [15] which contain the most general one-body information on proton structure. After integration over the spatial coordinates, they reduce to TMDs (see Fig. 1), and after integration over the transverse momentum and a specific Fourier transform they recover the GPDs [2, 3, 4].

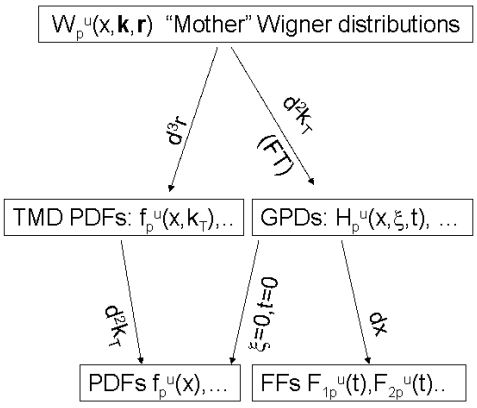

Figure 1: Wigner distributions. The f functions are the unpolarized PDFs, F_1 and F_2 are Dirac and Pauli elastic form factors and the kinematic variables ξ, t and k_T are the longitudinal and total momentum transfer and the transverse momentum of partons, respectively.

Single-Spin Asymmetries (SSAs) in azimuthal distributions of final state particles in semi-inclusive deep inelastic scattering play a crucial role in the study of transverse momentum distributions of quarks in the nucleon and provide access to the orbital angular momentum of quarks. Large SSAs, observed in hadronic reactions for decades [9, 10] have been among the most difficult phenomena to understand from first principles in QCD. Recently, significant SSAs were reported in semi-inclusive DIS (SIDIS) by the HERMES collaboration at HERA [11, 12, 13] for longitudinally and transversely polarized targets, and by the CLAS collaboration with a polarized beam [14].

SSAs are zero in the simplest treatments of the parton model and perturbative QCD. The asymmetries vanish for models of hadrons consisting of non-interacting collinear partons (quarks and gluons). This follows from the conservation of parity, total angular momentum, and the helicity of the individual quarks when applied in the Breit frame where the two interacting quarks reverse direction without exchanging energy. In perturbative QCD, which applied when the transverse momentum $P_\perp$ of the detected hadron is large compared to Λ_{QCD}, asymmetries vanish at the leading twist level. The observed single-spin asymmetries occur at $P_\perp$ below 1-2 GeV, which is not much larger than Λ_{QCD} or the typical parton transverse momenta of the order of 0.5 GeV. Thus the asymmetries could arise from non-collinear parton configurations or from multi-parton correlations ("higher twist" effects, which are suppressed at large $P_\perp$). Presently, the intrinsic transverse momentum of partons in the nucleon plays the crucial role in most explanations of non-zero single-spin asymmetries in polarized hadronic reactions. Two fundamental mechanisms have been identified leading to SSAs in hard processes, the Sivers mechanism [16, 17, 18, 19, 20, 21], which generates an asymmetry in the distribution of quarks due to orbital motion of partons, and the Collins mechanism [22, 7], which generates an asymmetry during the hadronization of quarks.

The HERMES Collaboration has recently measured a transverse spin asymmetry in SIDIS providing the cleanest evidence to date for the existence of a non-zero Collins function [13], which describes the fragmentation of a transversely polarized quark into pions. This finding is supported by the preliminary data from BELLE [23] indicating a significant Collins effect. The large target SSA in semi-inclusive pion production measured at CLAS [24] and analyzed in terms of the Collins fragmentation [25], also indicate a significant Collins function. The simple assumption that hadronization of quarks into hadrons is spin-independent appears to be false. High statistics data from this proposal can definitely confirm this.

CLAS target SSAs were measured using the 5.7 GeV data from the EG1 experiment using a polarized NH_3 target [26]. The twist-2 Mulders distribution function $h_{1L}^\perp$ was extracted for the first time using the π^+ target SSA [27], which is less sensitive to the unknown ratio of unfavored (d-quark fragmenting to π^+) to favored (u-quark fragmenting to π^+) polarized fragmentation functions. The π^+ sample, however may have a significant contribution from exclusive ρ^0 production, which is one of the largest

sources of systematic uncertainties in SIDIS measurements. So far, no evidence has been found with CLAS for the large unfavored Collins fragmentation indicated by HERMES. Current statistical errors for π^- and in particular π^0, which is relatively free of possible higher twist contributions [28], are large and do not allow strong conclusions from the measured SSAs. This proposal relies on the enhanced capabilities for detection of small angle photons to increase the sample of π^0s by a factor of 20 and therefore make possible the extraction of x, z and $p_\perp$ dependences of the target SSA. These measurements are essential for the study of polarized fragmentation process and will provide the first significant measurement of π^0 asymmetries.

We propose a measurement of single and double spin asymmetries in SIDIS using the CLAS in Hall B at Jefferson Lab, a 6 GeV longitudinally polarized electron beam, a longitudinally polarized proton (NH_3) target and the Inner Calorimeter. We propose to run with high luminosity, $1.5{\times}10^{34}$ cm^{-2}s^{-1}, yielding an integrated luminosity of 7.5×10^7 nb^{-1}.

2 Theory and motivation

2.1 Phenomenology of the TMDs

The major breakthroughs in the theoretical understanding of transverse distributions in the last two years include:

- Understanding the role of partonic initial and final state interactions [29, 19, 20]
- Proving factorization for SIDIS at low transverse momenta [30]
- Proving universality of the TMD correlation functions, including the sign change for two T-odd TMD distributions between Drell-Yan and DIS [19, 31]

As shown recently in Ref. [29, 19, 20, 21, 32], the interaction between the active parton in the hadron and the spectators leads to gauge-invariant TMDs. Furthermore, QCD factorization for semi-inclusive deep inelastic scattering at low transverse momentum in the current-fragmentation region has been established in Refs. [30, 31]. A detailed verification of factorization and calculations of the relevant factors in the factorization formulas have also been carried out in Ref. [30]. This new framework provides a rigorous basis to study the TMD parton distributions from SIDIS data using different spin-dependent and independent observables. TMD distributions (see Table 1) describe transitions of a nucleon with one polarization in the initial state to a quark with another polarization in the final state. The diagonal elements of the table are the momentum, longitudinal and transverse spin distributions of partons, and represent well-known PDFs related to the square of the leading-twist light-cone

Table 1: Leading twist transverse momentum dependent distribution functions. The U,L,T stand for transitions of unpolarized, longitudinally polarized and transversely polarized nucleons (rows) to corresponding quarks (columns).

N/q	U	L	T	
U	$\mathbf{f_1}$			$h_1^\perp$
L		$\mathbf{g_1}$		$h_{1L}^\perp$
T	$f_{1T}^\perp$	g_{1T}	$\mathbf{h_1}$	$h_{1T}^\perp$

wave functions. Off diagonal elements require non-zero orbital angular momentum and are related to the wave function overlap of L=0 and L=1 Fock states of the nucleon [33]. In particular, $f_{1T}^\perp$ and $h_1^\perp$, related to the imaginary part of the interference of wave functions for different orbital momentum states and known as the Sivers and Boer functions [16, 17, 18, 19, 20, 21], describe unpolarized quarks in the transversely polarized nucleon and transversely polarized quarks in the unpolarized nucleon respectively. They are *time-reversal odd* (T-odd) and can only be nonzero when initial or final state interactions cause an interference between different helicity states.

Another important quantity accessible in SSA measurements is the Mulders leading-twist distribution function $h_{1L}^\perp$. It is related to the real part of the interference of wave functions for different orbital momentum states, and describes transversely polarized quarks in the longitudinally polarized nucleon. Similar quantities arise in the hadronization process. One particular case is the Collins T-odd fragmentation function $H_1^\perp$ [22] which gives the probability of a transversely polarized quark fragmenting into unpolarized hadrons.

2.2 Factorization in SIDIS

The SIDIS cross section at leading twist has eight contributions related to different combinations of the polarization state of the incoming lepton and the target nucleon [6, 30].

$$\begin{aligned}\frac{d\sigma}{dxdydz_h d^2\vec{P}_{h\perp}} &= \tfrac{4\pi\alpha_{\rm em}^2 s}{Q^4}(1-y+y^2/2)xF_{UU}^{(1)} - (1-y)x\cos(2\phi_h)F_{UU}^{(2)} \\ &+\lambda S_L y(1-y/2)xF_{LL} + S_L(1-y)x\sin(2\phi_h)F_{UL} \\ &+|S_T|(1-y+y^2/2)x\sin(\phi_h-\phi_S)F_{UT}^{(1)} \\ &+|S_T|(1-y)x\sin(\phi_h+\phi_S)F_{UT}^{(2)} \\ &+\lambda|S_T|y(1-y/2)x\cos(\phi_h-\phi_S)F_{LT} \\ &+\tfrac{1}{2}|S_T|(1-y)x\sin(3\phi_h-\phi_S)F_{UT}^{(3)}] \end{aligned} \quad (1)$$

The kinematic variables x, y are defined as: $x = Q^2/2(P_1 q)$, and $y = (P_1 q)/(P_1 k_1)$. The variable $q = k_1 - k_2$ is the momentum of the virtual photon, $Q^2 = -q^2$, ϕ_h is the azimuthal angle between the scattering plane formed by the initial and final momenta of the electron and the production plane formed by the transverse momentum of the observed hadron and the virtual photon (see Fig. 2), ϕ_S is the azimuthal angle of the transverse spin in the scattering plane. The subscripts in F_{UL}, F_{LL},etc., specify the beam (first index) and target(second index) polarizations, longitudinal (L), transverse (T), unpolarized (U),

Structure functions factorize into TMD parton distributions and fragmentation functions, and into soft and hard parts [30]

$$\begin{aligned}
\sigma_{UU} \propto F_{UU} \propto \quad & f_1(x, k_\perp)\, D_1(z_h, p_\perp)\, S(\vec{\ell}_\perp) H_{UU}(Q^2) \\
\sigma_{LL} \propto F_{LL} \propto \quad & g_{1L}(x, k_\perp)\, D_1(z_h, p_\perp)\, S(\vec{\ell}_\perp) H_{LL}(Q^2) \\
\sigma_{UL} \propto F_{UL} \propto \quad & h_{1L}^\perp(x, k_\perp)\, H_1^\perp(z_h, p_\perp)\, S(\vec{\ell}_\perp) H_{UL}(Q^2),
\end{aligned} \tag{2}$$

where $z = (P_1 P_h)/(P_1 q)$, $k_\perp$ and $p_\perp$ are quark transverse momenta before and after scattering, and P_1 and P_h are the four momenta of the initial nucleon and the observed final-state hadron respectively.

The unpolarized D_1 and polarized $H_1^\perp$ fragmentation functions depend in general on the transverse momentum of the fragmenting quark.

S_L and S_T are longitudinal and transverse components of the target polarization with respect to the direction of the virtual photon. The different hard factors (H_{UU}, H_{LL},etc.), which are calculable in pQCD, in the SIDIS cross section are similar at one-loop order [30] and may cancel to a large extent in asymmetry observables. The soft factor $S(\vec{\ell}_\perp)$ comes from soft gluon radiation and is defined by a matrix element of Wilson lines in the QCD vacuum [30]. With a certain choice of factorization parameters, the soft factor could become unity. This may explain the success of existing phenomenology, based on the "naive" factorization assumption [7].

In the case of the polarized beam and target the cross section has contributions that depend on the spin of the target or the spin of the beam or both and involve all 8 leading twist TMD distribution functions [7, 39, 8, 40].

For a longitudinally polarized target the only azimuthal asymmetry arising in leading order is the $\sin 2\phi$ moment.

$$\sigma_{UL}^{\sin 2\phi} \quad \propto \quad S_L 2(1-y) \sin 2\phi \sum_{q,\bar{q}} e_q^2 x h_{1L}^{\perp q}(x) H_1^{\perp q}(z), \tag{3}$$

The physics of σ_{UL}, which involves the Collins fragmentation function $H_1^\perp$ and Mulders distribution function $h_{1L}^\perp$, was first discussed by Kotzinian and Mulders in 1996 [7, 6, 41]. The same distribution function is accessible in double polarized Drell-Yan, where it gives rise to the $\cos 2\phi$ azimuthal moment in the cross section [42].

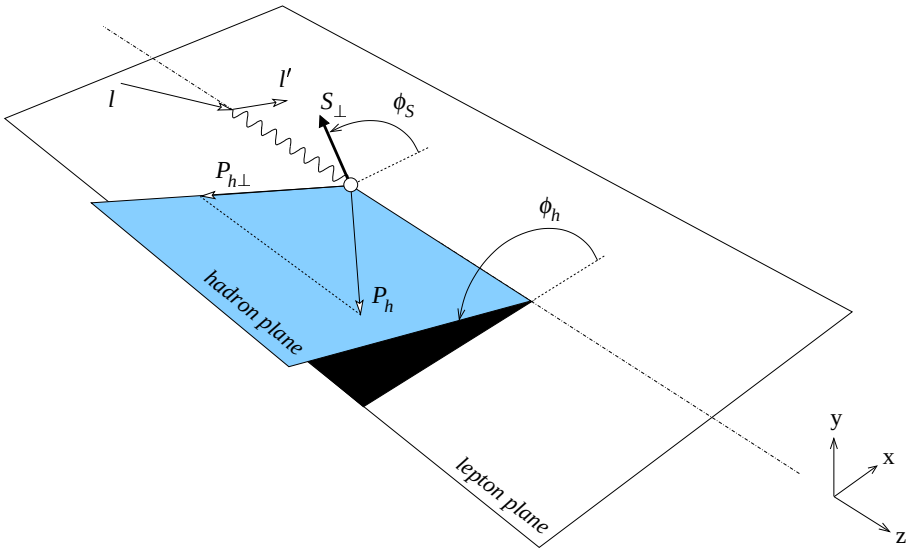

Figure 2: SIDIS kinematics. For a longitudinally polarized target, ϕ_S=0 or 180^o for negative and positive helicities of the proton, respectively.

The SIDIS cross section with a longitudinally polarized target in sub-leading order contains an additional contribution to the $\sin\phi$ moment (σ_{UL}). This asymmetry [41, 8, 45] first observed by the HERMES collaboration [11] involves the Collins fragmentation function $H_1^\perp$ and the twist 3 distribution function h_L [43]:

$$\sigma_{UL}^{\sin\phi} \quad \propto \quad S_L \sin\phi\,(2-y)\sqrt{1-y}\frac{M}{Q}\sum_{q,\bar{q}} e_q^2 x^2 h_L^q(x) H_1^{\perp q}(z). \tag{4}$$

It has been shown that h_L and $h_{1L}^\perp$ can be related by the integral equation [7, 33].

$$h_L = -\frac{1}{xM^2}\int k_\perp^2 h_{1L}^\perp d^2k_\perp$$

The function h_L is one of three basic higher twist distribution functions that is non-zero after integration over transverse momentum. It can also be measured through the Drell-Yan process with transversely-polarized protons scattering on longitudinally polarized protons [43].

Neglecting the contribution from the transverse component $A_\perp$, which is suppressed kinematically and therefore small [44], the double spin dependent contribution become a simple function of g_1:

$$\frac{d^2\sigma_{LL}}{dx\,dQ^2} \quad = \quad \lambda S_L \frac{4\pi\alpha^2}{Q^4}\left(y(2-y)g_1(x,Q^2)\right), \tag{5}$$

The ratio of spin dependent and spin independent cross sections for the longitudinally polarized target is defined by the ratio of structure functions $g_1(x,Q^2)$ and $F_1(x,Q^2)$

$$A_{||} = \frac{g_1(x,Q^2)}{F_1(x,Q^2)} D'(y), \tag{6}$$

where the kinematic (depolarization) factor is given by

$$D'(y) = \frac{y(2-y)}{y^2 + 2\left(1 - y - \frac{y^2\gamma^2}{4}\right)\frac{(1+R)}{(1+\gamma^2)}}, \tag{7}$$

$R(x,Q^2)$ is the ratio of the longitudinal and transverse photo absorption cross sections and $\gamma^2 = 4M^2x^2/Q^2$.

3 Experimental situation

3.1 Factorization studies at JLab

Because the average energy available for current quark fragmentation is rather low with a 6 GeV electron beam, it is not obvious whether semi-inclusive electroproduction can be factorized into a product of quark distribution functions and favored and unfavored fragmentation functions. The validity of factorization is crucial to the interpretation of target SSAs in terms of TMDs, which is the main goal of this proposal. We therefore present some of the recent evidence that factorization is valid in the kinematics of this proposal.

An experiment in Hall C (E00-108) recently investigated the kinematic where experimental data appear to satisfy the factorization hypothesis. The experiment consisted of scattering unpolarized electrons from unpolarized proton and deuteron targets, and detecting scattered π^- or π^+ in coincidence with scattered electrons in DIS kinematics ($W > 2$ GeV, $Q^2 > 2$ GeV^2). Three experimental tests using preliminary data support factorization in the region $0.2 < x < 0.6$ for $Q^2 > 2$ GeV^2, $0.3 < z < 0.7$, and $P_\perp < 0.5$ GeV (data were not taken at higher $P_\perp$). On the other hand, a clear break down of factorization was observed for $z > 0.7$ [47]. The first test examined the ratio of π^+ to π^- production from deuterium, which is expected to depend in LO QCD only on the ratio of favored and unfavored fragmentation functions. This ratio was found to have the z dependence expected from fragmentation functions determined at a much higher beam energy at HERMES, and to be independent of x and $P_\perp$ for $z = 0.55$, as expected if factorization holds. The second and third tests involved the study of the proton to deuteron ratio of the the sum and difference of π^+ and π^- production rates. In LO QCD and ignoring

sea quark contributions, fragmentation functions cancel in both of these ratios, which should therefore be independent of z and $P_\perp$, and have the x-dependence observed in inclusive scattering determinations of u and d quark distribution functions. The ratios for $x = 0.3$ indeed are independent of z up to $z = 0.7$, beyond which the ratios change dramatically, and are independent of $P_\perp$ in the region studied ($P_\perp < 0.5$ GeV). The x-dependence of both ratios closely follows that expected from the GRV PDF parametrization at $z = 0.55$. Overall, the Hall C data provide good support for factorization in the kinematic region of this proposal.

Unpolarized data from CLAS also support factorization, which predicts that the pion multiplicity (fraction of electron events with a pion observed at a given value of z) should be independent of x. As can be seen in the left panel of Fig. 3, CLAS data with a 5.7 GeV electron beam support this hypothesis in the (x, Q^2) range of the present proposal for $0.3 < z < 0.7$.

It is also possible to examine factorization using double-spin SIDIS data. It is worthwhile to look at factorization with the additional spin degree of freedom, because the additional selectivity introduced by spin may delay the onset of factorization to higher values of Q^2 and W than for spin-averaged scattering. There are in fact preliminary indications that this may be the case in the related phenomenon of quark-hadron duality in inclusive scattering in the resonance region [34].

For spin-dependent SIDIS studies, we use CLAS data collected as a by-product during the Eg1b run in the year 2000 with a 5.7 GeV longitudinally polarized electron beam incident on an NH_3 longitudinally polarized target. The average beam polarization was 0.73 ± 0.03 and the average target polarization was 0.72 ± 0.05. The CLAS acceptance [46] at 5.7 GeV covers a wide range of kinematics in the deep inelastic scattering domain (W $\geq$ 2 GeV and $Q^2 \geq 1$ GeV^2). The open acceptance of CLAS and a single electron trigger ensured event recording for a large sample of SIDIS π^+, π^0, and π^- events. In addition to the double spin asymmetry ($A_{1p}^{\pi+/-/0}$) measurements, target SSA measurements were also made.

The double polarization asymmetry A_1 is measured by counting the sum and difference of events with anti-parallel ($\lambda = 1$,$S_L = 1$) and parallel ($\lambda = 1$,$S_L = -1$) spin states of beam and target:

$$A_1 = \frac{1}{f D'(y) P_e P_t} \frac{N^{+-} - N^{++}}{N^{+-} + N^{++}},$$

where f is the dilution factor, P_e and P_t are beam and target polarizations and $D'(y)$ is the depolarization factor (see Eq. 7).

A first factorization test comes from examining the z-dependence of the Eg1b double spin asymmetries for all three pion flavors, as shown in the right panel of Fig. 3. The data cuts included $W > 2$ GeV and $Q^2 > 1.1$ GeV^2 to ensure DIS kinematics, and the average value of x is approximately 0.3, as in the Hall C experiment (although the range is larger, covering $0.15 < x < 0.5$). If factorization holds, the asymmetries should be approximately independent of z, broken by the different weights given to

the polarized u and d quarks by the favored and unfavored fragmentation functions. We therefore expect the largest z-dependence for the π^- asymmetries. This is indeed born out by the data, which are in excellent agreement in both magnitude and z-dependence up to $z = 0.7$ with predictions of the polarized Lund Monte Carlo using GRSV polarized PDFs as input.

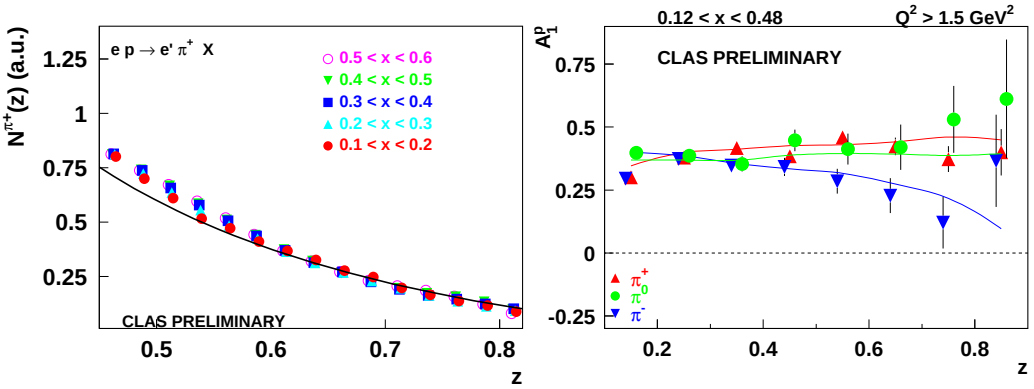

Figure 3: The multiplicity of SIDIS π^+ for different x-bins (left) and the double spin asymmetry from data compared to LUND-MC (curves) as a function of z. The preliminary data are from CLAS with a 5.7 GeV electron beam.

The $P_\perp$-dependence of the double-spin asymmetry was also studied for different bins in z and x to test the factorization hypothesis and possible transition to the perturbative limit, where the asymmetry is expected to be independent of $P_\perp$ [30]. The measured double-spin asymmetry (see Fig. 4) indeed is consistent with a constant, both for data averaged over z (left panel), as well as for individual z-bins (right panel) doesn't show any significant structure. This is contrast to the $P_\perp$-dependence of SSAs measured at HERMES [11] and CLAS [14] (see Fig. 8, right panel), which are expected to be $P_\perp$ dependent because they are not integrated over ϕ, as is the case for the double-spin asymmetries, and therefore sensitive to the magnitude of $P_\perp$.

The dependence of the double spin asymmetry on Bjorken x for different pion flavors obtained from the Eg1 data and the LUND-MC for the same kinematic range is presented in Fig. 5. The CLAS double polarized asymmetry A_1 is consistent with HERMES semi-inclusive data (Fig. 5) at fives times higher beam energy and three times higher Q^2, indicating no significant Q^2 dependence of the double polarized asymmetry A_1. An examination of the CLAS data on it's own indicates significant Q^2 dependence only for $Q^2 < 1$ GeV^2 (not shown in the figure). The π^0 double spin asymmetry as well as A_1^p for the sum of charged pions are consistent with the inclusive A_1^p as expected in a simple partonic picture (see Fig. 5).

All of these studies strongly suggest that factorization works for $W > 2$ GeV, $Q^2 > 1.1$ GeV^2, $0.15 < x < 0.5$, and $0.3 < z < 0.7$ for a 6 GeV electron energy.

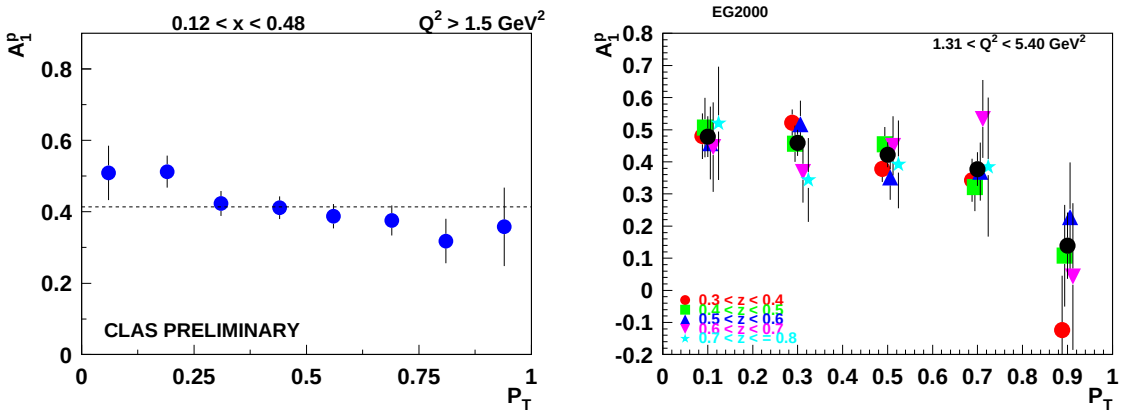

Figure 4: Comparison of A_1^p for π^+ as a function of $P_\perp$ (GeV) for different z and Q^2 ranges. Filled circles are for the average in the $0.4 < z < 0.7$ range.

The improved statistical accuracy of this proposal for inclusive and SIDIS scattering for all three pion flavors will permit much more detailed and quantitative studies of factorization in spin-dependent electron scattering.

3.2 Leading twist SSA in SIDIS with polarized target and beam

Measurements of average moments $\langle W(\phi)\rangle_{UL} = \int \sigma_{UL}(\phi) W(\phi) d\phi / \int \sigma(\phi) \sin^2\phi d\phi$ ($W(\phi) = \sin\phi, \sin 2\phi$) of the cross section $\sigma_{UL}^{W(\phi)}$ will single out corresponding terms in the cross section. Thus the $\sin\phi$ SSA of the cross section for longitudinally polarized beam and unpolarized target is defined as:

$$A_{LU}^{\sin\phi} = \frac{\langle \sin\phi \rangle_{LU}}{\langle \sin^2\phi \rangle_{UU}} = \frac{1}{P^\pm N^\pm} \frac{\sum_{i=1}^{N^\pm} \sin\phi_i}{\sum_{i=1}^{N^\pm} \sin^2\phi_i}, \tag{8}$$

where $P^\pm$ and $N^\pm$ are the polarization and number of events for $\pm$ helicity state, respectively. For spin-dependent moments this is equivalent to the corresponding spin asymmetries A_{UL}^W. The final asymmetry is defined by the weighted average over two independent measurements for both helicity states or by fitting with corresponding azimuthal dependences ($\sin\phi, \sin 2\phi$) the spin asymmetries binned in the azimuthal angle.

A unique feature of the Collins mechanism is the presence of a leading twist $\sin 2\phi$ SSA for a longitudinally polarized target [41]. Measurements of the $\sin 2\phi$ SSA (see Figs. 6 and 8) thus allow the study of the Collins effect with no contamination from other mechanisms. A recent measurement of $\sin 2\phi$ moment of σ_{UL} by HERMES [11] is consistent with zero. A measurably large asymmetry has been predicted only at

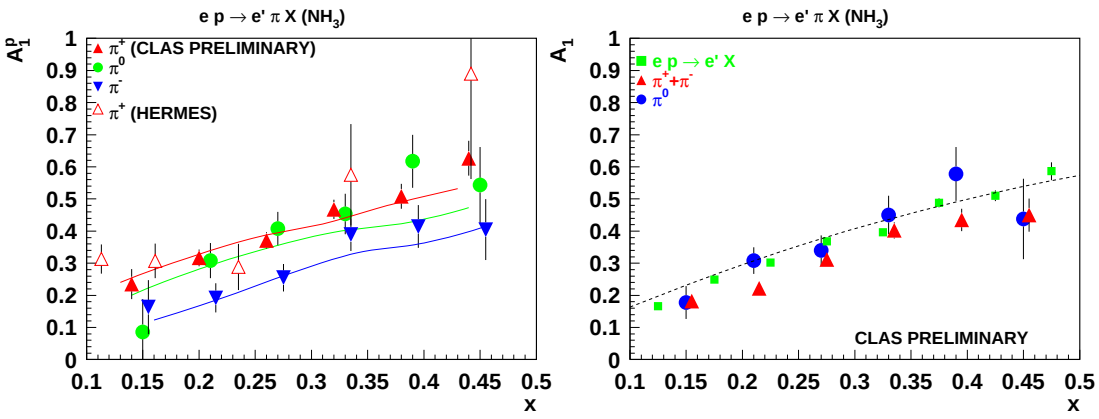

Figure 5: The double spin asymmetry as a function of x from an NH_3 target for different pion flavors. Open triangles correspond to the HERMES measurement of A_1^p for π^+ [48]. The right plot shows the comparison of inclusive A_1^p with the A_1^p for the sum of π^+ and π^- and A_1^p for π^0.

large x ($x > 0.2$), a region well-covered by JLab [35]. The leading-twist distribution function $h_{1L}^{\perp}(x)$, accessible in this measurement, describes the transverse polarization of quarks in a longitudinally polarized proton.

The $\sin 2\phi$ asymmetry from CLAS Eg1 is plotted in Fig. 6 as a function of x and z. The x dependence of the SSA for π^+ is consistent with predictions [49] and the z dependence is consistent with an increasing difference from zero as expected for the Collins function. The π^+ SSA is dominated by the u-quarks; therefore with some assumption about the ratio of unfavored to favored Collins fragmentation functions, it can provide a first glimpse of the twist-2 Mulders TMD (Fig. 7.) The curve is the calculation by Efremov et al. [49], using $h_{1L}^{\perp}$ from the chiral quark soliton model evolved to Q^2=1.5 GeV^2. The extraction, however, suffers from low statistics and has a significant systematic error from the unknown ratio of the Collins favored and unfavored fragmentation functions, the unknown ratio of h_{1L}^d/h_{1L}^u, as well as from background from exclusive vector mesons. More data are required for a statistically significant measurement of the $\sin 2\phi$ moment.

3.3 Subleading twist SSA in SIDIS with polarized target and beam

The $\sin\phi$ moment of the cross section measured with CLAS at 5.7 GeV is in agreement with the HERMES measurement at 27.5 GeV for a longitudinal target [11], indicating a bigger asymmetry for the higher twist contribution compared to the leading twist $\sin 2\phi$ moment.

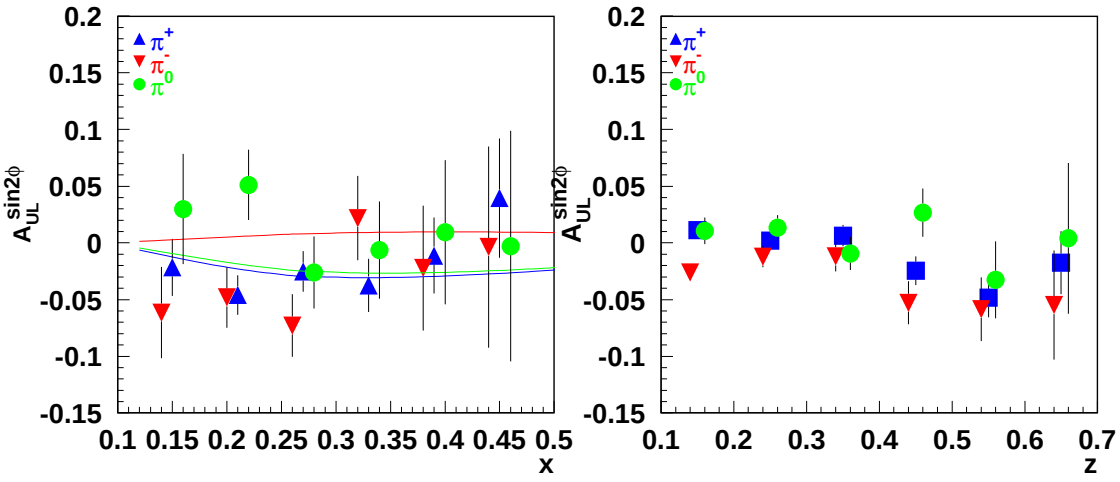

Figure 6: The leading twist SSA for the $\sin 2\phi$ moment for π^+, π^0, and π^- as a function of x (left plot) and z (right plot). The curves are from [49] using the χQSM calculations of $h_{1L}^{\perp}$

The $P_\perp$ dependence of the $\sin\phi$ moment for π^+ (see Fig. 8) is consistent with an increase with increasing $P_\perp$, as expected for the TMD function [30]. The $\sin\phi$ moment, for π^- is also plotted in Fig. 8, showing first evidence for a non-zero SSA asymmetry for π^- on a longitudinally polarized target.

The $\sin\phi$ moment of the SIDIS cross section itself can be an important source of independent information on the Collins fragmentation mechanism. The $\sin\phi$ moments of the SIDIS cross section with a longitudinally polarized target may contain contributions both from the Sivers effect [16] and the Collins effect [22], although latest HERMES measurements indicate that the Sivers contribution to the longitudinal SSA is negligible. A small contribution from the Sivers effect was confirmed also from different phenomenological studies [59, 60].

It is important to note, that both π^+ and π^- SSAs may have significant contributions from exclusive vector meson production. The fraction of π^+ in the single pion sample, coming from exclusive ρ^0 decays is somewhat less, but still significant at large z and in particular for small x. Fig. 9 shows the fraction of π^+ coming from ρ^0 decays extracted from the PYTHIA-MC. More data are required to extract exclusive two pion asymmetries and estimate their contribution to single pion SSA.

3.4 Multihadron final states

The large kinematic and geometric acceptance of the CLAS detector will let us accumulate a significant sample of two pion final states. Significant target-spin asymme-

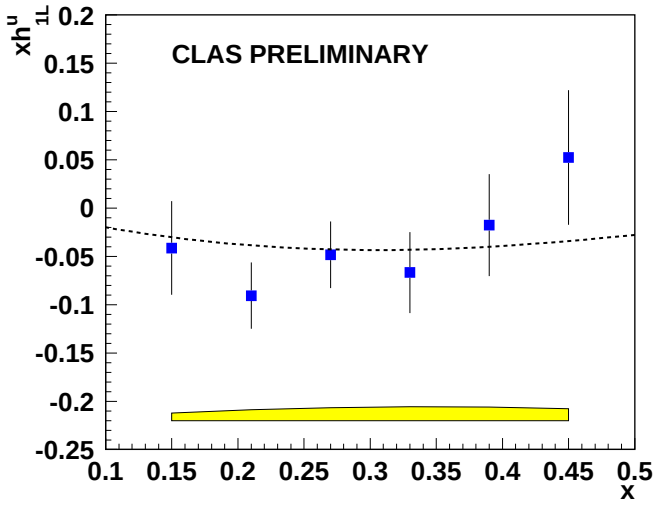

Figure 7: Mulders distribution functions from the π^+ SSA from Eg1 data. The contribution from the unfavored production is included in the systematic error band. The variation for the ratio of unfavored to favored Collins functions is from -2.5 to 0.

tries in semi-inclusive two-pion production were measured recently by the HERMES experiment, using a longitudinally polarized deuterium target [61]. Two-pion final states access the transversity distribution function and interference fragmentation functions [61, 62, 63]. They are also important in studies of the background to SIDIS pions. The contributions from exclusive two-pion events in general, and diffractive ρ^0 in particular, may have an important impact on SIDIS observables [64]. The preliminary Eg1b results for A_1 for exclusive ρ^0 production are plotted in Fig. 10as a function of W for four Q^2 bins [65]. The error bars at large Q^2 however are too big to make any conclusions on the possible effect on SIDIS pions. The errors will shrink by about a factor of three to four with data collected from the presently proposed experiment.

3.5 Inclusive and semi-inclusive DIS

Inclusive and semi-inclusive double-spin asymmetries will not only be valuable for factorizaation studies, as outlined above, but will also be of considerable interest for the improved knowledge of polarized PDFs that they will provide.

By measuring the double-spin inclusive asymmetry $A_1(x)$ at large x, one can test different predictions about the limit of $A_1(x)$ as $x \to 1$. Non-relativistic Constituent Quark Models (CQM) based on SU(6) symmetry predict $A_1(x) = 5/9$ at all x for the proton, $A_1(x) = 0$ for the neutron and $A_1(x) = 1/3$ for the deuteron (modified by its D-state). Quark models that include some mechanism of SU(6) symmetry breaking (*e.g.*, one–gluon exchange hyperfine interaction between quarks [52]) predict that

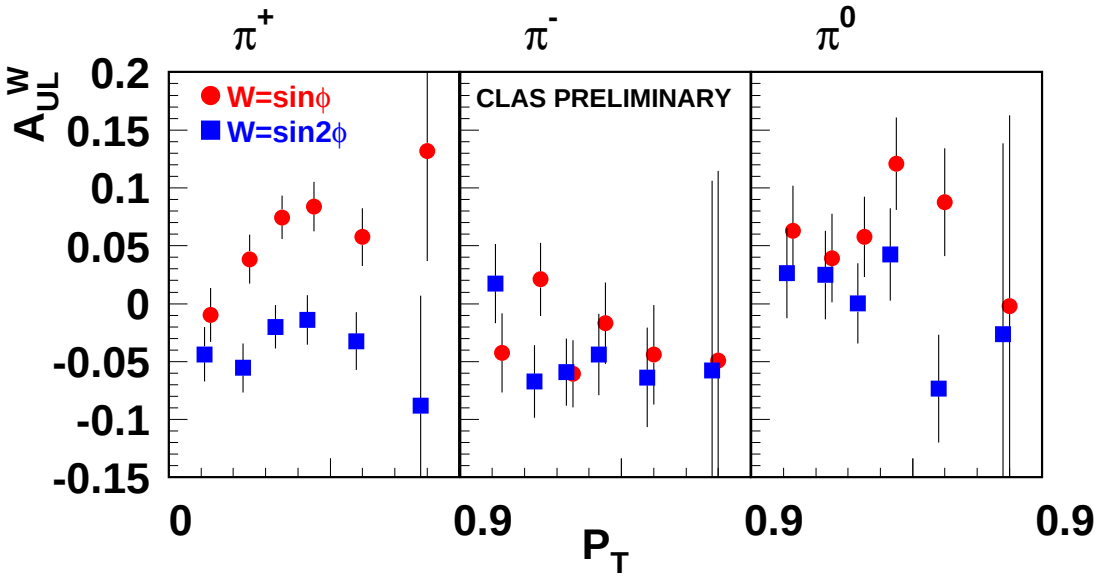

Figure 8: The A_{UL} SSA dependence on $P_\perp$.

$A_1(x) \to 1$ for all three targets as x tends to 1, since target remnants with total spin 1 are suppressed relative to those with spin 0. The same limit for $x \to 1$ is also predicted by pQCD [53], where hadron helicity conservation suppresses the contribution from quarks anti–aligned with the nucleon spin. However, in this case the approach to $A_1(x) = 1$ would be faster since both u and d quarks contribute with positive polarization. Finally, a recent paper [54] connected the behavior of $A_1(x)$ at large x with the dynamics of resonance production via duality, leading to several predictions for the approach to $A_1(x) = 1$, depending on the mechanism of SU(6) symmetry breaking one assumes.

The double spin asymmetry in SIDIS for charged and neutral pions is sensitive to the polarized parton densities through the different flavor sensitivities tagged by the pion charge. Since it is now possible to include SIDIS in NLO QCD analysis, quantitative tests of the factorization approach can be done within this framework to find regions of consistent fits in specific ranges of kinematic variables. This can be done by χ^2 tests as in Ref. [57, 58]. Our expectation is that consistent NLO QCD fits

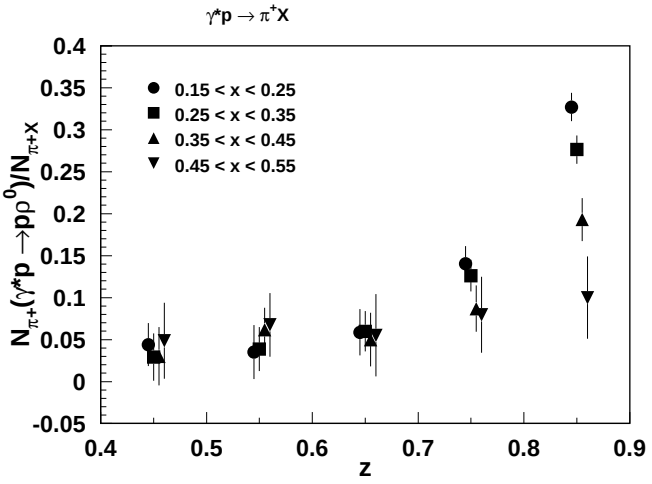

Figure 9: Fraction of π^+ coming from ρ^0 decays as a function of z for different x-bins.

will be possible for $0.15 < x < 0.5$, $Q^2 > 1.3$ GeV^2, $M_x > 1.4$ GeV, $0.3 < z < 0.7$, and $P_\perp < 1$ GeV. The improved precision from the data of the present proposal will allow to determine if some corners of this space show marked deviations from a smooth NLO QCD fit, due to complications such as higher twist effects, diffractive ρ^0 production, or target fragmentation.

In terms of improved parton densities, an important observation is that the systematic errors largely cancel in the ratio of g_1/F_1 for SIDIS pion production to the values for inclusive production. Therefore this ratio, which is unity in LO QCD for π^0 or the sum of π^+ and π^- if sea quark contributions and gluon radiation are ignored, can be measured with high statistical and systematic precision (for example with relative errors of 3% in each of 5 x bins). The deviations from unity which are expected due to different sea quark contributions and gluon radiation in the evolution equations can therefore be determined with unprecedented accuracy.

3.6 Related JLab proposals

The approved Hall C experiment E04-113 will measure SIDIS π^+, π^-, K^+, and K^- from polarized protons and deuterons over kinematics similar to Eg1 and this proposal. The main focus of that experiment is to measure the double spin asymmetry, although the target SSA will also be measured on one side of the q vector (hence limiting the coverage in the out-of-plane angle ϕ). It is hoped that measurements of the transverse double spin asymmetry and target SSA can also be made for the

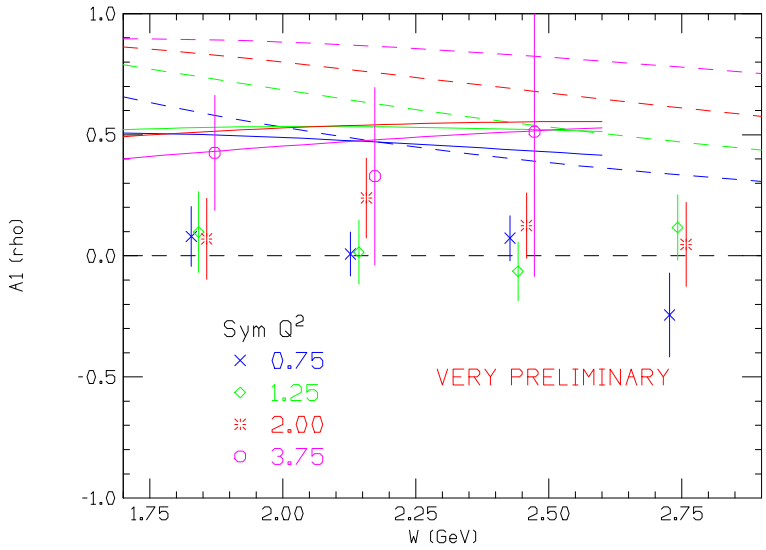

Figure 10: $A_1(\rho)$ for $ep \to p\rho^0$ as a function of W, averaged over $0 < -t' < 0.4$, for four bins in Q^2. The solid curves are from Kochelev *et al.* [66] and the dashed curves are from Fraas [67]. The data points increase with Q^2 from left to right, and the dashed curves increase with Q^2 from bottom to top.

proton with the same apparatus during the E03-109 experiment (SANE), which will complement the present proposal, for which only a longitudinally polarized target will be used. In contrast to the Hall C experiments, the SIDIS part of the present proposal focuses on the π^0 state. The separation of $\sin\phi$ and $\sin 2\phi$ moments requires a wide coverage in ϕ accessible only at CLAS. The full azimuthal coverage and high statistical accuracy, which will permit measurements of the target SSAs with unprecedented systematic and statistical precision makes it unique.

3.7 The HERMES experiment

The HERMES collaboration has published the first data on the SSA with a longitudinally polarized target [11]. These results are consistent with zero. However they suffer from a rather low luminosity and low average z. Moreover, the asymmetry is predicted to be large only at large x, not accessible at HERMES with currently available data set. The HERMES collaboration currently has no plans for more longitudinally polarized target runs.

3.8 The COMPASS experiment

The COMPASS experiment at CERN is running 80% of its time with a longitudinally polarized target. The signal however is not expected to be strong enough in their kinematics, in particular for the deuteron target, to measure a significant SSA [49].

4 A dedicated experiment in Hall B

The main goal of the proposed experiment is to measure the kinematic dependence of the $\sin 2\phi$ moment of the target spin-dependent cross section. This will be the first statistically significant measurement of kinematic dependences for a TMD distribution. The $\sin\phi$ moment will also be studied to establish the twist-3 and twist-2 nature of the $\sin\phi$ and $\sin 2\phi$ moments (from their Q^2 dependence), and to establish the existence and magnitude of the Collins fragmentation function through the dependence on hadron fractional energy z.

In addition, the experiment will yield superior measurements of double spin asymmetries in inclusive DIS and SIDIS for single pion production, providing high statistics data for NLO analysis of polarized parton densities. These data will also be used to further elucidate the kinematic range for which factorization of quark distributions and fragmentation functions is valid. This is of crucial importance, as the interpretation of the $\sin 2\phi$ and $\sin\phi$ dependence of SIDIS relies on the factorization hypothesis.

Measurements of single and double spin asymmetries for two-pion final states, including semi-inclusive and exclusive ρ production will probe transversity and interference fragmentation functions as well as providing important information for background studies in single pion semi-inclusive production.

4.1 Overview of the experiment

We propose to scatter high energy longitudinally polarized electrons from polarized protons in a low temperature dynamically polarized NH_3 target. The scattered electrons and photons from π^0 decay will be detected with the CLAS, enhanced by the new Inner Calorimeter (IC). The open small angle geometry of the polarized target makes it well-matched to the IC. Without the IC a significant portion of the photon yield is lost at small angles.

The GEANT MC developed for the Eg1 [56] experiment was used to study the proposed experiment, a layout of which is shown in Fig. 11. The kinematic coverage for neutral pions obtained with the MC is shown in Fig. 12. The simulated π^0 detection efficiency is shown in Fig. 13, from which it is seen that use of the IC will increase the π^0 detection efficiency relative to previous CLAS measurements by a factor of 2 to 4, with the improvement largest for high energy pions.

Although the main focus of the proposed experiment is the study of single and double spin asymmetries of π^0's, the accumulated sample of π^+ and π^- will increase the size of the existing event sample by nearly an order of magnitude. In this regard we note that the IC will block the acceptance of high energy charged particles below 15°. The simulated acceptance for π^+ is shown in Fig. 14. Although the charged pions blocked by the IC are not included in our projections, some of them will pass through the IC and will be detected in the CLAS. GSIM studies are underway to estimate this fraction and the efficiency for their reconstruction. The detection of π^-

is especially important for SSA studies and measurements of diffractive ρ^0 production.

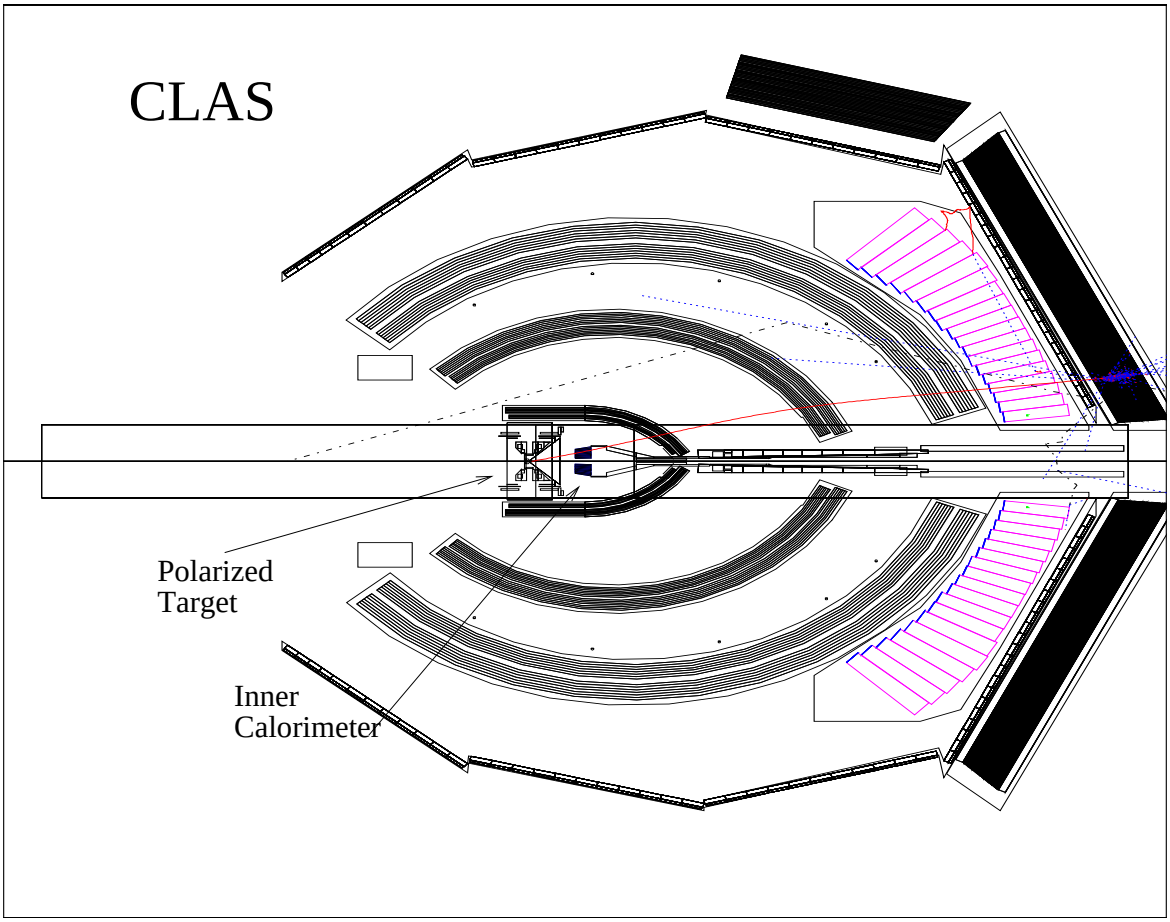

Figure 11: Polarized target and the inner calorimeter (IC) in the GEANT simulation. The pion track at 12° is shown passing through the IC.

4.2 Beam requirements: energy and polarization

The proposed study of single and double polarization asymmetries requires the highest available energy and longitudinal polarization for the incoming electrons. The highest possible beam energy provides the greatest access to the hard scattering kinematic region ($Q^2 > 1$ GeV^2 and $W^2 > 4$ GeV^2). High beam polarization is required for the double spin asymmetry studies, which are an important part of the proposed semi-inclusive program. Projections for measurements were done assuming a beam energy of 5.75 GeV, a beam polarization of 80% and total beam time of 60 days (50 days on NH_3, the remainder used for background and polarimetry measurements, and for target changes).

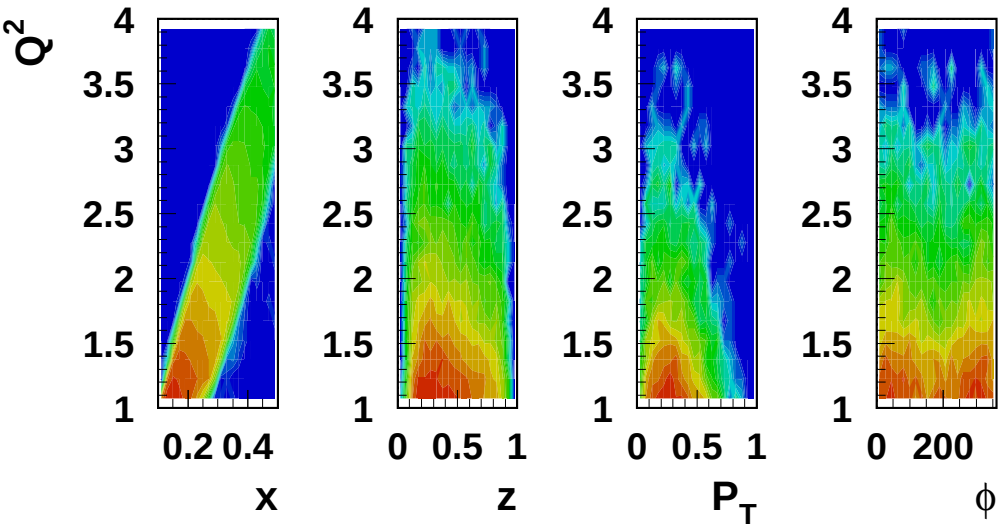

Figure 12: The accessible range of Q^2, x_B, z and $P_\perp$ with CLAS for a 6 GeV beam with a π^0 measured in the final state. Simulations were done for torus current $I_T = 2250$ A and for the Eg1 standard configuration (target position $Z_{trg} = -55$ cm.)

4.3 The CLAS, polarized target and Inner Calorimeter

4.3.1 The CLAS longitudinally polarized target

For this proposed experiment, we use the same target setup as in the Eg1 run and the approved experiment E-03-006 [72]. The setup consists of a target insert which holds four target cells that can be moved by means of a stepping motor into the beam. The target materials are polarized solid ammonia ($^{14}NH_3$), ^{12}C and an empty cell. Since, unlike Eg1, we will not use deuterated ammonia in this experiment, both of the instrumented target cups will be filled with ($^{14}NH_3$), maximizing the time each insert can be used without annealing or changing material. The ammonia target is polarized via Dynamic Nuclear Polarization, which requires cooling the target to 1 K, and holding it in a uniform ($\Delta B/B = 10^{-4}$) magnetic field of 5T. The holding field is

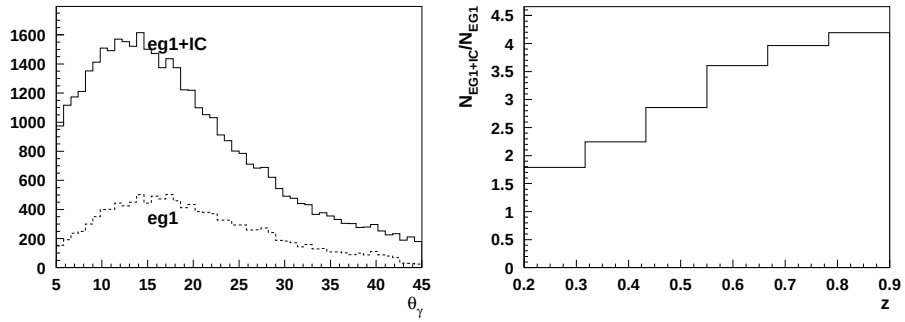

Figure 13: GEANT simulation for π^0 photon acceptance in polar angle of the energetic photon (left) and z (right) comparing the Eg1 configuration with and without IC.

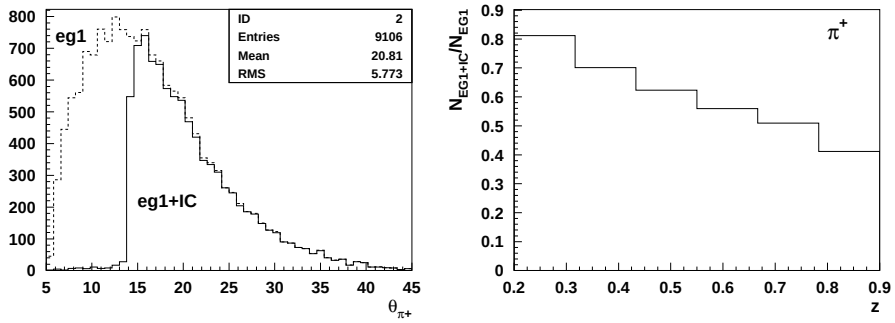

Figure 14: Same as Fig 13 for π^+

supplied by two superconducting Helmholtz-like coils placed axially around the target. The target polarization direction will be reversed many times during the experiment by changing the frequency of the microwaves used to polarize the target. The cooling system is a ^{4}He evaporation refrigerator. The ^{4}He, N, and Al endcap contributions to the cross sections and asymmetries will be determined using data from the ^{12}C and empty cell targets. Approximately 7 days of running on these targets will be needed for accurate measurements of the dilution factor and background asymmetries.

We expect target polarizations of about 70-90%, as were achieved in the Eg1b experiment. The target polarization will be continuously monitored with an NMR system for prompt feedback on the optimum polarizing microwave frequency, and to determine when to anneal the target to recover the polarization lost due to radiation damage. For a more accurate determination of the product of target and beam polarizations, P_eP_t, we will use the well-known ep elastic scattering asymmetry, as was done in Eg1b. For a longitudinally polarized target, this asymmetry is quite insensitive to the ratio of elastic form factors G_E^p/G_M^p, so that the error on P_eP_t will

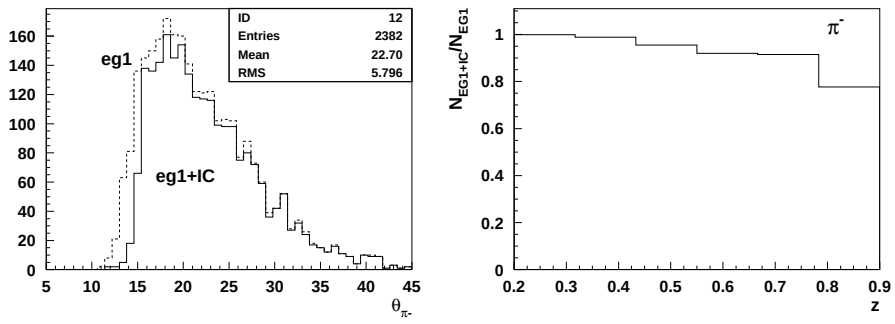

Figure 15: Same as Fig 13 for π^-

be dominated by the statistical errors of about 2% per target orientation. For the determination of the average target polarization in each orientation, we will divide P_eP_t determined from *ep* elastic scattering by P_e determined to a relative accuracy of approximately 3% from periodic beam polarization measurements using the Hall B Møller polarimeter.

To minimize radiation damage to the target the beam will be rastered over the target surface in a spiral pattern. The beam motion is indirectly recorded in the data stream by storing the ADC values of the raster magnet.

The polarized target magnetic field shields the detector from the Møller electrons produced in the target by focusing them onto the beam line. Møller electrons, which are the vastly dominating source of electromagnetic background, will pass through the central penetration in the lead-tungstate wall, and be absorbed in the downstream shielding pipe. The shielding arrangement is very similar to the one used during Eg1.

The minimum angle for the detection of high energy photons in the proposed configuration is approximately 6°. Although the polarized target allows detection of lower angles than available with unpolarized target with a mini-torus, the forward acceptance of CLAS forward calorimeter limits the photon detection.

The IC designed for the e1-DVCS experiment, used with polarized target will significantly increase the kinematic coverage for the direct detection of high-energy photons from the decay of high momentum π^0. The polarized target centered at -55 cm (as in Eg1) allows the installation of the DVCS photon detector within the Region I drift chamber region, while maintaining sufficient angular resolution to separate single photons from $\pi^0 \to \gamma\gamma$ events (see Fig. 16). This setup was studied in detail during a recent test run and the optimal running conditions were identified.

4.3.2 Inner Calorimeter

A new electromagnetic calorimeter (IC), was built for the experiment E-01-113 [74] to measure the DVCS beam single spin asymmetries. Its coverage of photons at

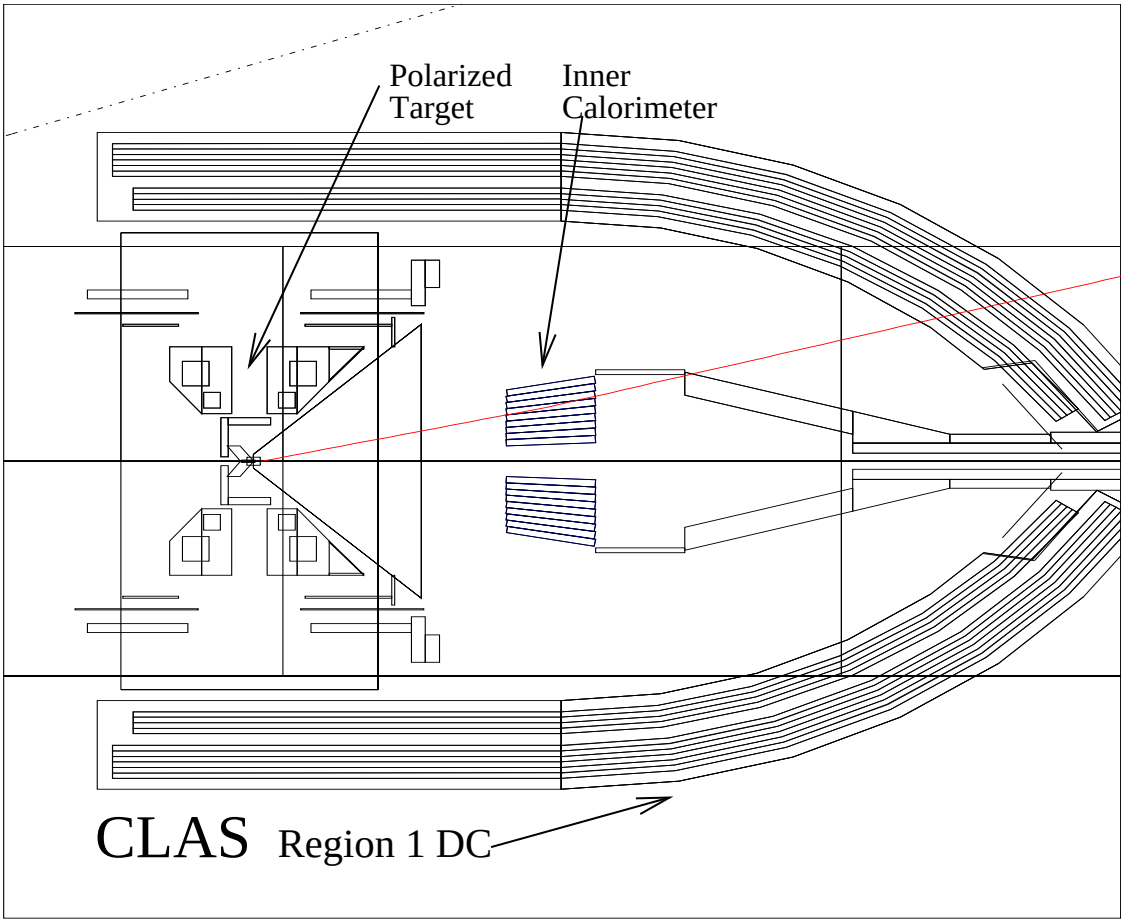

Figure 16: CLAS arrangement proposed for this measurement. Region I is shown with the polarized target (left) and the DVCS inner calorimeter (IC, right). The red line is a typical high energy π^- passing through the IC

small angles (4-15 degrees) ideally complements the standard CLAS electromagnetic calorimeter (EC) and is well matched to the detection of high energy photons.

The IC was built in 2003-2004 by a ITEP/JLab/Orsay/Saclay collaboration, and was operated successfully during the spring of 2005 for the first part of the e1-DVCS run [74] (a 100-crystal prototype was tested in the fall of 2003, in a configuration relevant to this proposal, which uses the polarized target magnet for shielding of Møller electrons).

A schematic of IC assembly is presented in Figure 16. The design benefited from R&D for the LHC-CMS experiment, but the IC is innovative in the significantly smaller crystal size, its mechanical assembly and the preamplifiers. The IC is composed of

- 424 lead tungstate ($PbWO_4$) tapered crystals, 160 mm long (18 radiation lengths), of section 13 mm$\times$13 mm to 16 mm$\times$16 mm,
- light detection through avalanche photo-diodes,
- low-noise (about 7-8 MeV) fast preamplifiers, allowing a software threshold at 15 MeV/crystal,
- specially designed mechanical structure minimizing the gaps between crystals,
- a thermal stabilization around 17°C within $\pm$ 0.02°C (both the crystal light output and the APD gain vary with temperature, resulting into a signal output variation of about 5%/°C),
- a laser system, used for tests and for monitoring of the relative gains as a function of time,
- standard associated read-out electronics (splitters, Fastbus ADCs - 200 ns gate width - and multi-hit TDCs).

It will be placed $\sim$ 60 cm in front of the target center.

Background and radiation damage

The background rates due to Møller electrons were simulated and then measured with the polarized target magnet (Helmholtz coils) during the prototype test. While the inner ring of crystals close to the beam axis exhibit a pile-up probability of 40-50%, with an exponentially decreasing energy distribution of mean 30-40 MeV, this probability falls to about 5-8% in the second ring and becomes negligible at larger angles. Correspondingly, the radiation dose was estimated to about 50 rad/hour in the inner layer, down to less than 0.1 rad/hour as of the fourth ring from the beam axis. Only the inner ring exhibited some sign of radiation damage (loss of approximately 10% in signal height) during 70 days of operation of e1-DVCS.

Energy resolution

From GEANT simulations of photon showers [71], an energy resolution of

$$\frac{\sigma_E}{E} = \frac{0.034}{E(\mathrm{GeV})} \oplus \frac{0.038}{\sqrt{E(\mathrm{GeV})}} \oplus 0.022$$

was determined. The first term corresponds to the preamplifiers noise. The second term is interpreted as fluctuations on the lateral containment of showers, plus a photostatistics contribution corresponding to 2000 photoelectrons per GeV. The third term is interpreted as fluctuations on energy leakage from the back of the crystals, plus a relative error in the gain calibration. Results from e1-dvcs π^0 calibrations (see below) indicate that the achieved resolution is better than anticipated:

$$\sigma_{M_{\pi^0}} \simeq 7.2 \text{ MeV} \Rightarrow \frac{\sigma_E}{E} \simeq 4\% \text{ at 1 GeV}$$

Position resolution

The position resolution has also been estimated from simulations [71]:

$$\sigma_x \simeq \frac{2.6 \text{ mm}}{\sqrt{E}} \oplus 0.3 \text{ mm} \quad .$$

This is consistent with the observed π^0 mass resolution from two photon events. At the planned position, 60 cm downstream from the production target, this corresponds to an angle resolution of approximately 3 mr at 2 GeV. This position resolution, together with an optimized cluster-finding algorithm, is sufficient to separate photons from π^0s up to 5 GeV.

The quality of energy and position reconstruction is illustrated using $ep \rightarrow ep\pi^0$ events from the e1-DVCS data set, comparing π^0 energy and angles calculated on one hand from $ep \rightarrow epX$ kinematics with $X = \pi^0$, on the other hand from the measured 2 photons in IC (see Figure 17).

Stability of the response

Lead-tungstate crystals are known to be rather sensitive in their light output to temperature changes. The ambient temperature during the e1-DVCS run was stabilized and monitored. The crystal/APD response was also carefully checked with light injected into the crystals via quartz fibers and the response recorded and used to monitor the gain.

Calibration

The crystal array will be calibrated in-situ using a method developed for the e1-DVCS run: specific runs will be taken with a high-multiplicity IC trigger. From

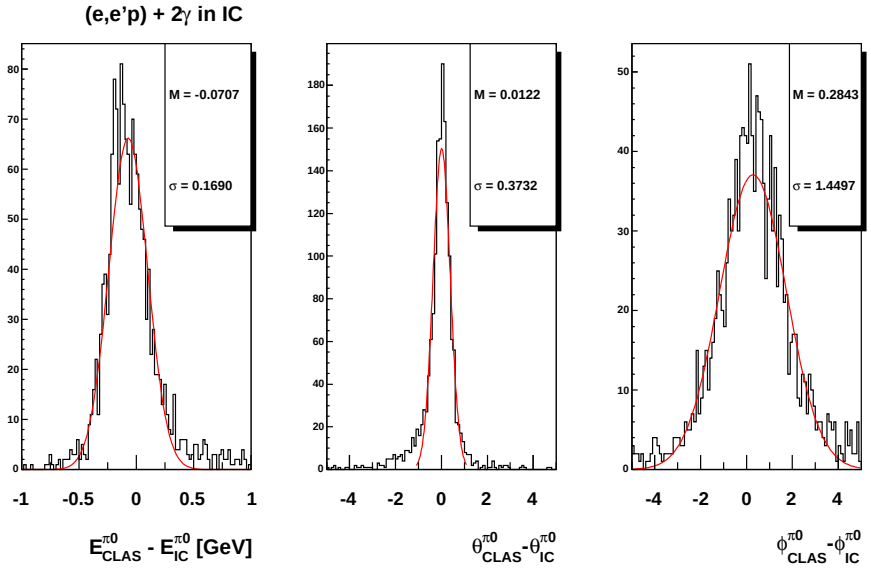

Figure 17: π^0 energy and angle reconstructions in the IC. The observed resolutions (in GeV and degrees) are a convolution of CLAS and IC resolutions.

these $\pi^0 \rightarrow \gamma\gamma$ events will be selected in IC, unrelated to particles detected in CLAS. An iterative procedure allows an adjustment of all individual gains which results in a minimization of the $\gamma\gamma$ invariant mass resolution. The quality of the π^0 mass reconstruction is illustrated in Figure 18, for $ep \rightarrow ep\pi^0$ events, where the two photons are detected either in the IC or the EC, or one photon is detected in each calorimeter. The IC is seen to have a resolution two times better than the EC.

4.3.3 Trigger and data acquisition

We are planning to use the standard EG1 production trigger, data acquisition, and online monitoring system of CLAS. The standard electron trigger consists of a time coincidence between the gas Cherenkov counter and the EC in a given sector. The signal amplitude and time information will be read out using standard ADC and TDC boards currently in use in CLAS. The crystal array information will be read out for every event, but not used in the trigger. The expected data acquisition rate is about 3 kHz, which can be handled by the DAQ with a reasonably small computer dead time. Additional pre-scaled triggers will be used to calibrate the Cherenkov and EC efficiencies for electrons.

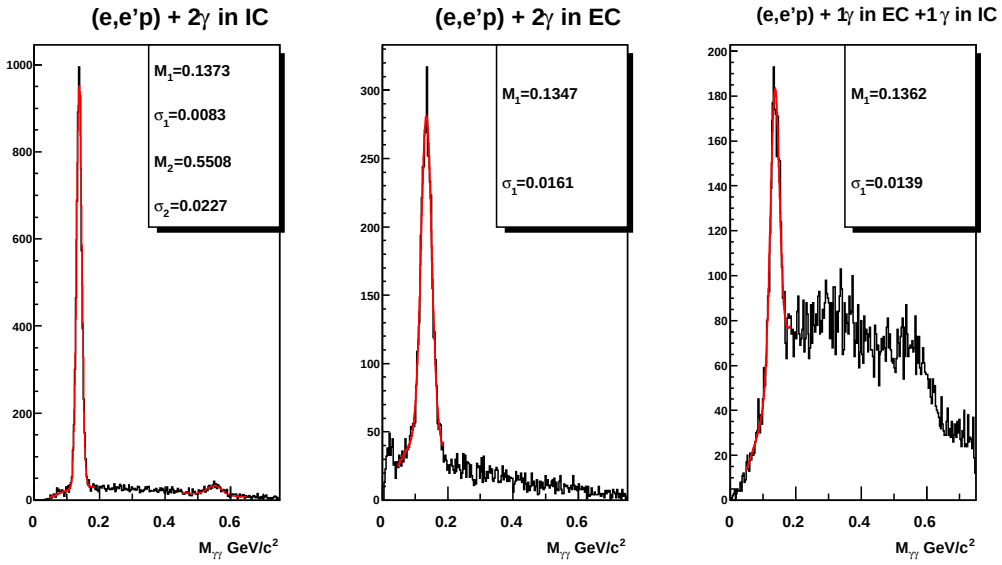

Figure 18: π^0 resolutions for different configurations. The left plot is for 2 photons in the IC, the middle one for 2 photons in the EC and the right one for mixed configurations.

4.3.4 Torus Polarity and Field Setting

We propose to run the bulk of the time with inbending (for electrons) torus polarity and a field setting of 2250 amps (2/3 of maximum). This field setting gives more than adequate momentum resolution for electrons for the measurements of this proposal. The inbending polarity optimizes the acceptance for $Q^2 > 1$ GeV^2 by a large factor, and also allows for running at higher luminosity (due to the higher trigger rate for the out-bending polarity).

Approximately 1 day of running will be needed with the out-bending polarity to measure the pair-symmetric background, which arises primarily from $\pi^0 \to \gamma e^+ e^-$ decays. Studies from Eg1 indicate that the typical e^+/e^- ratio is < 0.02 for SIDIS (largest at low x), and < 0.03 for inclusive g_1 for $x > 0.3$. Therefore 1 day of running time will be sufficient to measure both the rate and asymmetries for the lepton pair-symmetric backgrounds.

4.3.5 Event identification, reconstruction, acceptances

Event identification in CLAS is accomplished using charged particle tracking in the toroidal magnetic field, time-of-flight, and momentum information. Electrons are separated from heavier particles using threshold gas Cherenkov detectors, and electromagnetic calorimeters.

The left plot in Fig. 20 shows the Cherenkov signal C_{pe} (in units of photoelectrons)

on the vertical axis and the normalized calorimeter response (E/P) on the horizontal axis, for torus field 2250 A, corresponding to the in-bending electron configuration suggested for this experiment. It can be seen the both the gas Cherenkov and EC are needed for clean electron identification. The right plot in Fig. 20 shows the target vertex distribution for electron candidates along with the cuts used in the analysis ($-58 < z < -52$) cm. Events from target windows more than 3 cm from the target center can be eliminated cleanly. After application of raster corrections [75], more than 98% of electrons passed the vertex cut used in Eg1. Figure 19 show the z-vertex position before and after the raster correction for the Eg1b data set.

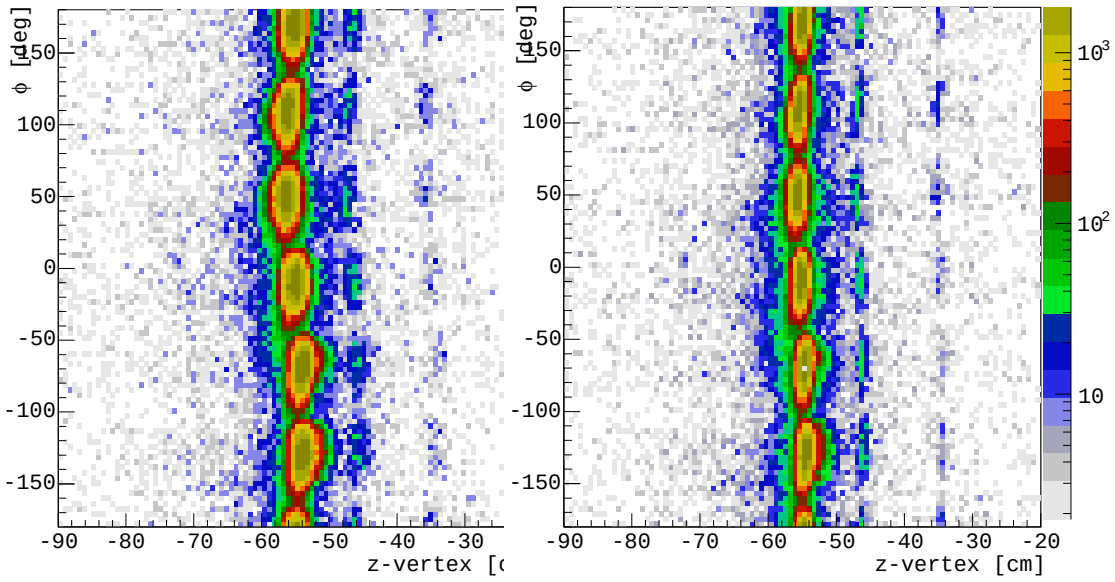

Figure 19: Electron z-vertex position for Eg1b data before and after the application of raster corrections

Charged hadrons are momentum-analyzed in the CLAS drift chamber system and are identified using the time-of-flight scintillators. The upper plots in Fig. 21 show the time difference (TOF) between the observed and expected arrival time for a charged pion of a given momentum, using the trigger electron to define the start time at the target. While pions and protons can be cleanly separated at all momenta, there is some kaon contamination in the pion sample above a momentum of 1.5 GeV.

For the proposed experiment, photons from π^0 decays (or from η decays) will be reconstructed using the IC and the CLAS forward-angle EC. This will provide large acceptance coverage for both reactions.

Neutral pions are identified using their decay to two photons. Photons are separated from neutrons by requiring their velocity $\beta > 0.8$, as measured with the calorimeter time. Their energy is determined from the normalized calorimeter (IC or EC) energy. A neutral pion is identified if the invariant mass squared of the two photons passes the cut $0 < M^2_{\gamma\gamma} < 0.04$ GeV^2. As illustrated in Fig. 22, this cut

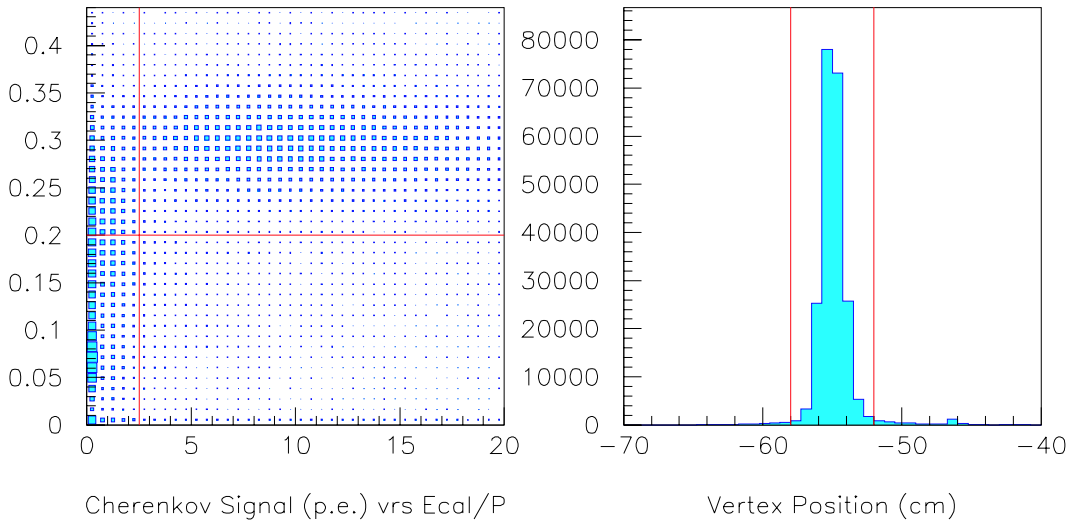

Figure 20: Left: Cherenkov signal versus normalized calorimeter energy for electron candidates. The cuts used for most events ($P < 3$) GeV are shown as the red lines. Right: reconstructed target position along the beam line for electron candidates.

identifies neutral pions with an efficiency of over 95%, while introducing $< 5\%$ of background in the forward calorimeter. The resolutions for the IC are shown in Fig. 18, and are about a factor of two better than for the EC.

4.4 Count rates and statistical errors

The expected number of counts is given by

$$N = \mathcal{L} \times \text{time} \times \sigma \times (\Delta Q^2 \cdot \Delta x_B) \times \Delta z \times \Delta P_\perp \times \Delta\phi \times \eta_{eff} \tag{9}$$

where the η_{eff} is the efficiency of reconstruction of particles.

The total number of expected events including all fiducial, data quality cuts as well as kinematic cuts was estimated using the existing Eg1 data. An additional scale factor accounting the change of the acceptance for different pion flavors due to the Inner Calorimeter was calculated using the LUND-MC and GEANT simulation of CLAS, reproducing well the eg1 data.

In a large acceptance detector like CLAS, the binning of the data according to the relevant kinematical variables is somewhat arbitrary. The data set will be summed over some number of bins, for a better study of the Q^2, x_B, z and $P_\perp$ dependences of the observables.

- The Q^2 and x_B bins are indicated in Table 3.
- The z range will be divided into 8 bins of width 0.1. The binning in $P_\perp$ will be in steps of 0.125 GeV.

Table 2: Uncertainties for asymmetry measurements.

Item	A_1^p	$A_{UL}^{\sin\phi}$	$A_{UL}^{\sin 2\phi}$
beam x target polarization	2%	-	-
target polarization	-	3%	3%
depolarization and R	5%	-	-
dilution factor	4%	4%	4%
radiative corrections	3%	3%	3%
fitting procedure	-	3%	5%
transverse (to γ^*) spin effects	5%	5%	-%

- The whole ϕ range will be divided into 12 bins of 30°.

This procedure would result in a total of 396 bins for the whole data set.

The number of events for 50 days of production running were calculated on the basis of existing Eg1 data and MC GSIM simulation of acceptances for different pions. Those numbers (see APPENDIX B) are used to calculate the statistical uncertainties illustrated in the figures of the following section. A target polarization of 0.8 is assumed for calculations of final error bars on plots, which also account for dilution and depolarization factors as well.

4.5 Systematic errors

The proposed spin asymmetry measurement is rather insensitive to uncertainties in acceptances and charge normalization. The main systematic error is due to possible contamination of the single pion sample with pions from decays of exclusive vector mesons. Other sources of systematic errors include the beam and target polarizations, dilution factor the longitudinal to transverse photoabsorption cross section ratio, $R(x, Q^2)$. The main sources of systematic errors in measurements of single and double spin asymmetries are listed in the Table 2. These errors are all scale errors, so are proportional to the size of the measured asymmetry. The total uncertainty is expected to be less than 10% of the measured SSA. For the $\sin 2\phi$ SSA, statistical uncertainties are expected to dominate the total uncertainty.

Studies of other sources of systematics, related to physics background, including target fragmentation, semi-exclusive processes, exclusive vector meson contributions and higher twist require the data of this measurement.

4.6 Projected results and impact on physics

Projections for some of the most important observables for 60 days of running with the proposed configuration are shown on Figs. 23-27. Fig. 23 shows the A_{UL} measured by eg1 for π^+, π^-, π^0 as a function of the azimuthal angle (open symbols). The error

bars for the filled symbols show the projected accuracy of this new measurement of the same asymmetry.

Projections for the resulting kinematic dependence of the leading twist SSA are shown in Fig. 24. Calculations were done using $h_{1L}^{\perp}$ from the chiral quark soliton model evolved to Q^2=1.5 GeV^2[49], f_1 from GRV95 [70], and D_1 from Kretzer, Leader and Christova[51]. Three different curves correspond to $H_1^{\perp u\to\pi^+}/H_1^{\perp u\to\pi^-} = 0, -1.2, -5$ [50]. The proposed measurement will pin down the TMD distribution and will constrain the ratio of favored and unfavored polarized fragmentation functions.

Projections for the resulting $P_\perp$ dependence of the $\sin\phi$ moment (higher twist SSA) are shown on Fig. 25. High-precision measurement will define whether the asymmetry is decreasing at large $P_\perp$, as predicted by pQCD [30]. This measurement is a complementary to leading twist information on the Collins fragmentation mechanism, and will test the predicted relationship between the leading-twist TMD $h_{1L}^{\perp}$ and the sub-leading higher-twist distribution h_L [43].

The new data will allow a more precise test of the factorization ansatz and the investigation of the Q^2 dependence of both $\sin 2\phi$ and $\sin\phi$ asymmetries. This will enable us to study the leading-twist and higher-twist nature of both observables.

Fig. 26 shows the SIDIS values of g_1/F_1 for the π^0 final state as a function of x, and the projected errors from the present proposal. While there there will be an overall scale error of approximately 6%, the point-to-point systematic errors are expected to be smaller or comparable to the statistical errors, allowing a greatly improved determination of the kinematic dependence of this asymmetry.

Fig. 27 shows the Eg1b results for inclusive A_1^p at high x, along with the projected errors from this proposal. For this plot, we have required $W > 2$ GeV to ensure DIS kinematics (which for $E = 6$ GeV ensures $Q^2 > 3$ GeV^2 for $x > 0.4$. The new data will significantly improve our knowledge of the x-dependence of A_1^p at high x, helping to distinguish between the many existing models. The proposed statistical error at $x = 0.6$ will be comparable to the systematic error (estimated to be the same as for Eg1b, as shown on the figure), and considerably smaller at lower values of x. Since the systematic errors are highly correlated from point-to-point (dominated by overall systematic errors), the x-dependence will be primarily determined by the statistical errors, while the overall magnitude of A_1 will be dominated by an overall scale factor uncertainty. The new data will help pin down the polarized u quark distribution with improved accuracy. When combined with high-statistics measurements of g_1^n (from a ^3He target in Hall A), this will also allow better determinations of the polarized d-quark distribution.

5 Summary and beam time request

In this experiment we propose a study of parton distributions and in particular TMD parton distributions using pion electroproduction in SIDIS for $Q^2 > 1$ GeV^2, a

6 GeV electron beam, the CLAS detector, the Eg1 polarized target and the e1-DVCS Inner Calorimeter.

For this proposal, we request new beam time of 60 days with highly polarized electrons at 6 GeV to access the large x region where the SSA due to Collins fragmentation is large. We expect smaller systematic uncertainties for π^0 double and single spin asymmetries than for charged pions. Using the increased capabilities for the direct detection of high energy photons at small angles in IC we expect an increase of the statistics by a factor of ~ 20 compared to existing Eg1 data.

The large kinematic and geometric acceptance of the CLAS detector will let us accumulate a significant sample of two-pion final states. Interesting in their own right [61, 62, 63], they are also important in studies of the background to SIDIS pions from exclusive two pions and ρ in particular.

We believe that the measurements we intend to carry out in this proposal are an indispensable prerequisite for the future development of the formalism of TMD parton distributions, an important component of the program covered by an energy upgraded JLab. This study involves a simultaneous scan of various variables (x_B, Q^2, z, $P_\perp$ and ϕ) and for that a large acceptance detector such as CLAS is most suitable. Analysis of already existing electroproduction data from the CLAS Eg1 experiment and studies based on simulations have shown that the proposed measurements are feasible.

The major improvement of projected error bars for pions for the dedicated measurement results from the increased acceptance for π^0 detection (~ 3), and longer running time (60 days). This will allow us to map out the x_B and z and $P_\perp$ dependence of both, single and double spin asymmetries of pions in smaller bins. The proposed measurement with CLAS will produce precision data on the single and double spin asymmetries in SIDIS, and will provide the first significant measurement of a twist 2 TMD parton distribution which will unlikely be superseded by any ongoing or planned experiments.

Beam Request

We ask the PAC to award 60 days of new beam time for a dedicated high statistics experiment to study pion production in SIDIS in hard scattering kinematics ($Q^2 > 1$, $W^2 > 4$).

The measurements involve the use of already existing equipment and the experiment could be ready to run within in a few months of approval. Precise data for SIDIS asymmetries at 6 GeV, produced in a timely fashion, will also help maintain the momentum in the theory community and help to support the program for the 12 GeV energy upgrade of CEBAF.

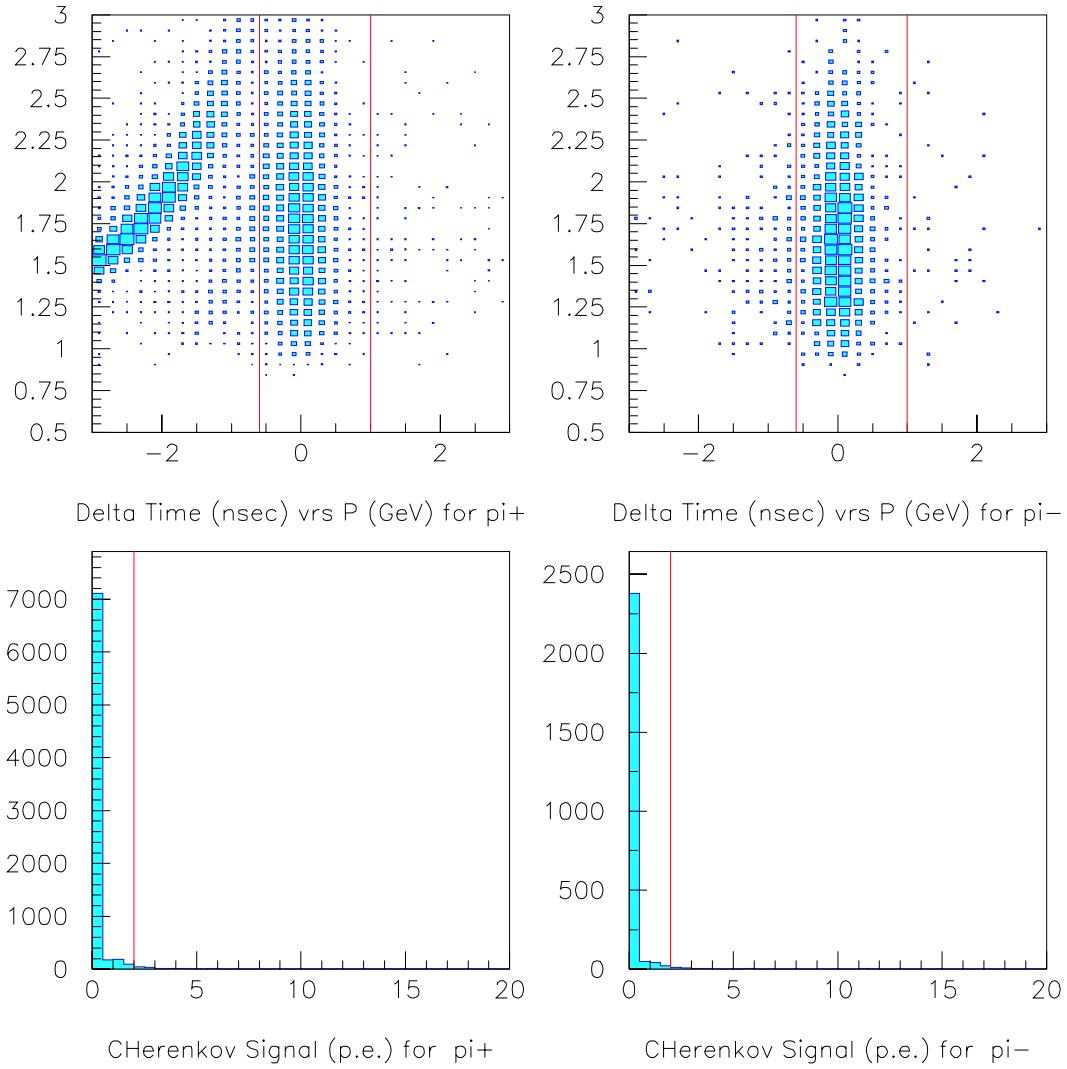

Figure 21: Upper: Time-of-flight difference from that expected for electron-pion coincidences as a function of momentum for positive (negative) hadrons on left (right). The red lines indicate the cuts used in the Eg1 analysis. Lower: Cherenkov counter signals for hadron candidates for positive (negative) hadrons on left (right)

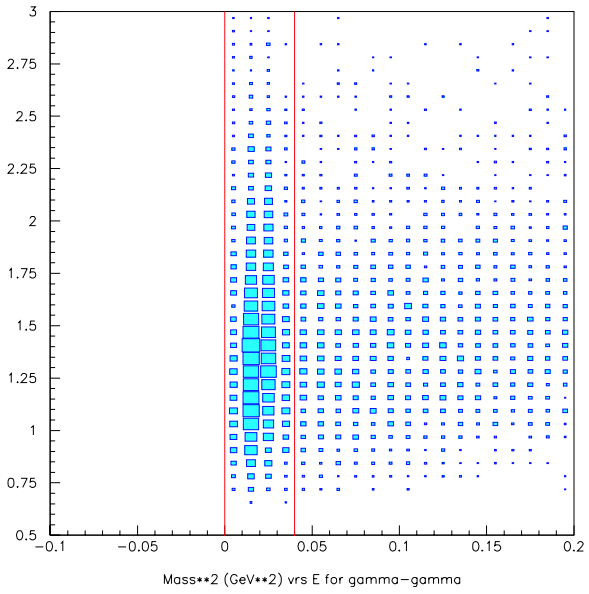

Figure 22: Invariant mass squared of two identified photons. The red lines indicate the cuts used to identify neutral pions in Eg1.

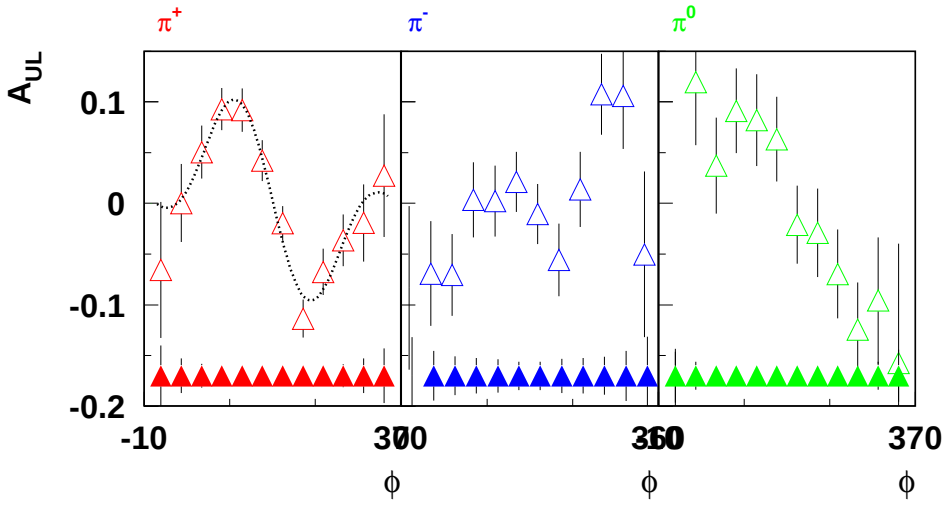

Figure 23: The target SSA as a function of the azimuthal angle ϕ from Eg1 data at 6 GeV for π^+, π^- and π^0. The open trangles represent the existing Eg1 data and filled triangles show the projected data.

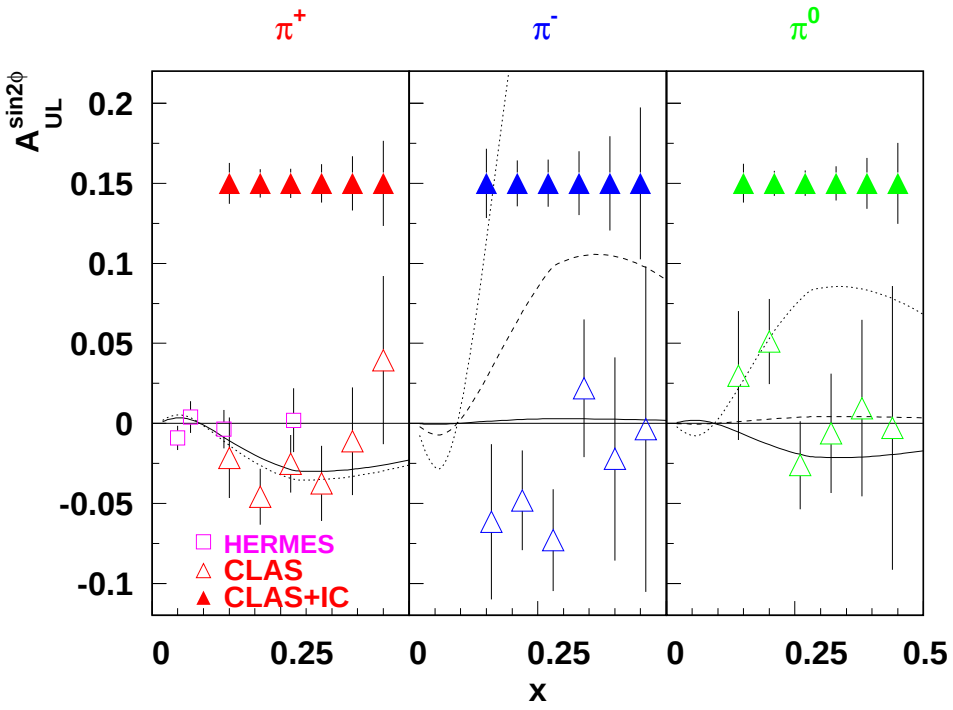

Figure 24: The x-dependence of the target SSA at 6 GeV. The points illustrate the expected statistical accuracy. The curves are calculated using [50].

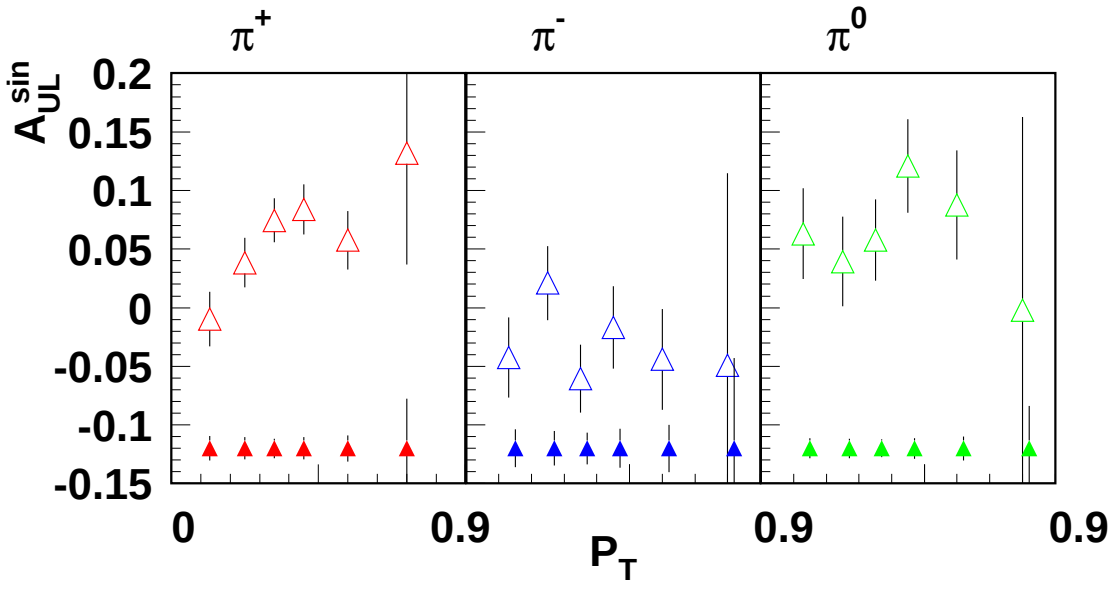

Figure 25: The $P_\perp$-dependence of the target SSA at 6 GeV from Eg1 data. The filled symbols show the expected statistical accuracy.

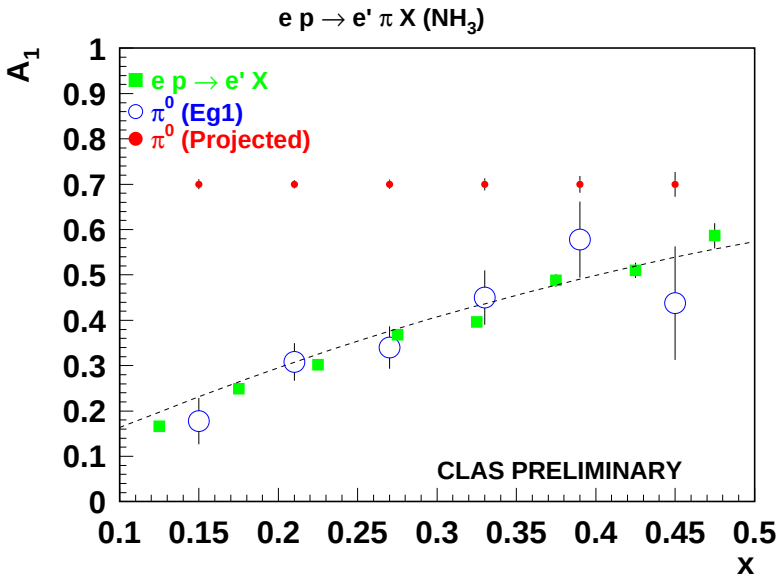

Figure 26: Preliminary Eg1b results for SIDIS $A_1 \approx g_1/F_1$ for π^0 as a function of x, and projected errors for this proposal. Also shown as the dashed line is the prediction using GRSV parton densities.

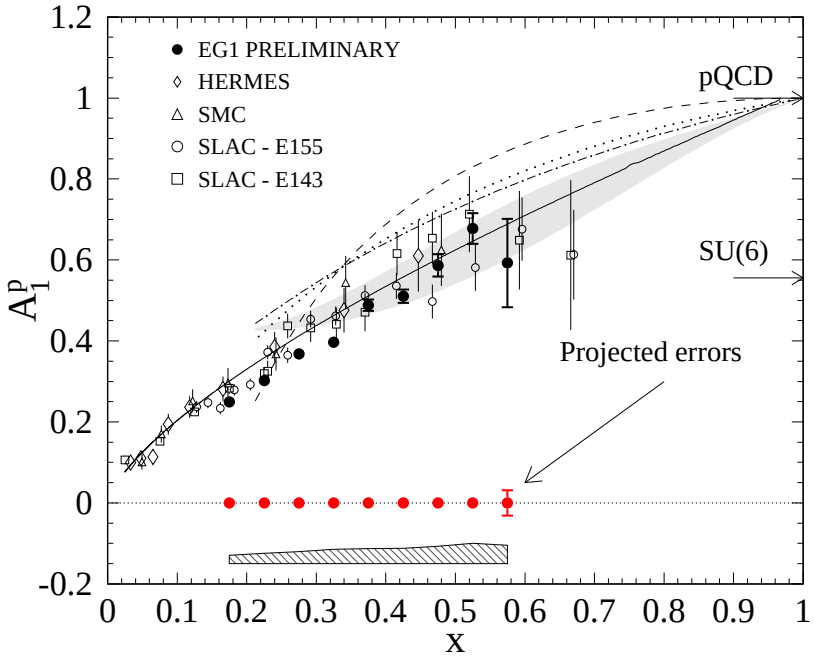

Figure 27: Results for the asymmetry $A_1(x)$ on the proton. Preliminary Eg1b data for $W > 2$ GeV (filled circles) are shown together with data from several previous experiments. The dashed line shows a parametrization of the world data at a fixed $Q^2 = 10$ GeV^2. The shaded band covers a range of calculations by Isgur [52] that model the hyperfine–interaction breaking of SU(6) symmetry. The remaining three curves correspond to different scenarios of SU(6) symmetry breaking as presented in the paper by Close and Melnitchouk [54].

References

[1] J. Ashman *et al.*, Phys. Lett. B **206**, 364 (1988).

[2] D. Muller *et al.*, Fortschr. Phys. **42**, 101 (1994).

[3] X. Ji, Phys. Rev. Lett. **78**, 610 (1997).

[4] A.V. Radyushkin, Phys. Lett. B **380**, 417 (1996).

[5] J. Ralston and D. Soper, Nucl. Phys. **B152**, 109 (1979)

[6] A. Kotzinian, Nucl. Phys. **B 441**, 234 (1995).

[7] P.J. Mulders and R.D. Tangerman, Nucl. Phys. **B461**, 197 (1996).

[8] D. Boer and P. Mulders, Phys.Rev. **D57**, 5780 (1998).

[9] K. Heller *et al.* 'Proceedings of Spin 96',Amsterdam,Sep.1996,p23

[10] Fermilab E704 collaboration (A. Bravar *et al.*), Phys.Rev.Lett. **77**, 2626 (1996).

[11] HERMES collaboration (A. Airapetyan *et al.*), Phys.Rev.Lett. **84**, 4047 (2000).

[12] HERMES collaboration (A. Airapetyan *et al.*), Phys.Rev. **D64**, 097101 (2001).

[13] HERMES collaboration (A. Airapetyan *et al.*), Phys.Rev.Lett. **94**, 012002 (2005).

[14] CLAS Collaboration (H. Avakian *et al.*) hep-ex/0301005.

[15] X. Ji, Phys. Rev. Lett. **91**, 062001 (2003); A. Belitsky, X. Ji and F. Yuan, Phys.Rev. **D69**, 074014 (2004).

[16] D. Sivers, Phys.Rev. **D43**, 261 (1991).

[17] M. Anselmino and F. Murgia, Phys. Lett. B **442**, 470 (1998).

[18] S. Brodsky *et al.*, Nucl. Phys. **B 642**, 344 (2002).

[19] J. Collins, Phys. Lett. B **536**, 43 (2002).

[20] X. Ji, F. Yuan, Phys. Lett. B **543**, 66 (2002).

[21] A. Belitsky,X. Ji and F. Yuan, Nucl. Phys. **B 656**, 165 (2003).

[22] J. Collins, Nucl. Phys. **B396**, 161 (1993).

[23] R. Seidl Proceedings of DIS-2005 (2005).

[24] H.Avakian,V.Burkert,L.Eloadrhiri Proceedings of SPIN-2004, Dubna Russia (2004).

[25] A. Efremov Annalen Phys. 13, 651 (2004)

[26] EG1 Collaboration.

[27] H.Avakian,P.Bosted,V.Burkert,L.Eloadrhiri Proceedings of DIS-2005 (2005).

[28] A. Afanasev *et al.*, Phys. Lett. B **398**, 393 (1997); Phys. Rev. D **58**, 054007 (1998); Phys. Rev. D **62**, 074011 (2000).

[29] S. Brodsky *et al.*, Phys. Lett. B **530**, 99 (2002).

[30] X. Ji, J-P. Ma and F. Yuan, e-Print Archive: hep-ph/0404183; Phys. Lett. B **597**, 299 (2004), e-Print arXiv: hep-ph/0405085.

[31] J. C. Collins and A. Metz, e-Print arXiv:hep-ph/0408249.

[32] D. Boer, P. J. Mulders and F. Pijlman, Nucl. Phys. B **667**, 201 (2003).

[33] X. Ji, J. P. Ma and F. Yuan, Nucl. Phys. B **652**, 383 (2003).

[34] W. Melnitchouk, R. Ent, C. E. Keppel, Phys. Rept. 406,127 (2005).

[35] A. Efremov *et al.*, Phys. Rev. D67, 114014 (2003).

[36] A. Afanasev and C. Carlson, hep-ph/0308163.

[37] A. Met and M. Schlegel, Eur. Phys. J. **A22**, 489 (2004)

[38] J. Collins and A. Metz, hep-ph/0408249 (2004).

[39] J. Levelt and P. J. Mulders, Phys. Lett. **B338**, 357 (1994).

[40] F. Yuan, Phys. Lett. B **589**, 28 (2004).

[41] A.M. Kotzinian and P.J. Mulders, Phys. Rev. D**54** 1229 (1996).

[42] R.D. Tangerman and P.J. Mulders, Phys.Rev. D**51** 3357 (1995).

[43] R.L. Jaffe and X. Ji, Nucl.Phys. **B375** (1992) 527.

[44] P.L. Anthony *et al.,*, The E155x Collaboration, Phys. Lett. **B 553**, 18 (2003).

[45] A. M. Kotzinian *et al.,* Nucl.Phys. **A666**, 290-295 (2000).

[46] B. Mecking *et al.*, Nucl. Instrum. Meth. **A503**, 513 (2003).

[47] R. Ent, talks given at Duality 2005 (http://www.lnf.infn.it/conference/duality05/) and JLab Users Meeting 2005 (http://www.jlab.org/ugm05/program.html)

[48] HERMES collaboration (A. Airapetyan *et al.*), Phys. Lett. B **562**, 182 (2003).

[49] A. V. Efremov, K. Goeke and P. Schweitzer, Phys. Rev. D **67** (2003) 114014 [arXiv:hep-ph/0208124].

[50] A. V. Efremov, K. Goeke and P. Schweitzer, Czech.J.Phys.(2005) [arXiv:hep-ph/0412420].

[51] Kretzer, Leader and Christova, hep-ph/0108055.

[52] N. Isgur, Phys. Rev. **D59**, 034013 (1999), hep-ph/9809255.

[53] G. R. Farrar and D. R. Jackson, Phys. Rev. Lett. **35**, 1416 (1975).

[54] F. E. Close and W. Melnitchouk, Phys. Rev. **C68**, 035210 (2003), hep-ph/0302013.

[55] M. Leberig, DIS 2004, Strbske Pleso, Slovakia, 14-18 Apr 2004.

[56] S. Chen, CLAS Analysis note (in preparation).

[57] A. Daleo and R. Sassot, Nucl. Phys. B673 (2003) 357, hep-ph/0309073

[58] A.N. Sissakian, O.Yu. Shevchenko, and O.N. Ivanov, hep-ph/0505012.

[59] A. Efremov *et al.* Phys. Lett. B568, 63 (2003).

[60] M. Anselmino et al. Phys. Rev. **D71**, 074006 (2005).

[61] P.B. van der Nat and K. Griffioen. hep-ex/0501009.

[62] R. L. Jaffe, X. Jin, and J. Tang, Phys. Rev. Lett. **80**,1166 (1998).

[63] A. Bacchetta and M. Radici Phys. Rev. **D 67**, 094002 (2003).

[64] M. Diehl, W. Kugler, A. Schaefer and C. Weiss hep-ph/0506171.

[65] P.Bosted, CLAS analysis note.

[66] N.I. Kochelev *et al.*, Phys. Rev. D **61**, 094008 (2000); Phys. Rev. D **65**, 097504 (2002); and private communication.

[67] H. Fraas, Nucl. Phys. **B113**, 532 (1976).

[68] J. Ellis, D. E. Kharzeev and A. Kotzinian, Z. Phys. **C69** 467 (1996).

[69] W. Melnitchouk and A. W. Thomas, Z. Phys. **A353** 311 (1996).

[70] M. Gluck *et al.*, Phys. Rev. **D53**, 4775 (1996).

[71] F.-X. Girod and M. Garçon, CLAS-Note-2005-001; R. Niyazov and S. Stepanyan, CLAS-Note in preparation.

[72] M. Battaglieri, R.De Vita, A. Deur, M. Ripani *et al.*, CEBAF experiment 03-006.

[73] M.K. Jones *et al.*, Phys. Rev. Lett. **84** (2000) 1398.

[74] V.D. Burkert, L. Elouadrhiri, M. Garçon, S. Stepanyan *et al.*, CEBAF experiment 01-113.

[75] P. Bosted, S. Kuhn, Y. Prok, CLAS-NOTE-03-008 (2003).

Appendix: Projected number of events for different bins

Table 3: Counts in bins in Q^2 and x_B, z and $P_\perp$.

x_B	Q^2 (GeV^2)	z	$P_\perp$ GeV	Counts π^+	π^-	π^0
0.15	1.31	0.35	0.06	34363	44	64575
0.15	1.31	0.35	0.19	158900	13662	339165
0.15	1.31	0.35	0.31	311731	109780	616050
0.15	1.31	0.35	0.44	369698	218603	714510
0.15	1.31	0.35	0.56	271159	222442	562410
0.15	1.31	0.35	0.69	150556	153340	312030
0.15	1.31	0.35	0.81	63665	73469	123075
0.15	1.31	0.35	0.94	21588	25344	30420
0.15	1.31	0.35	1.06	5026	6226	5625
0.15	1.31	0.45	0.06	18431	22	19215
0.15	1.31	0.45	0.19	81431	6853	97020
0.15	1.31	0.45	0.31	151116	42647	186615
0.15	1.31	0.45	0.44	191114	89078	259695
0.15	1.31	0.45	0.56	168420	92323	252540
0.15	1.31	0.45	0.69	105581	73942	183735
0.15	1.31	0.45	0.81	53235	44605	103590
0.15	1.31	0.45	0.94	22365	21505	45495
0.15	1.31	0.45	1.06	8596	8844	17910
0.15	1.31	0.55	0.06	11711	33	6120
0.15	1.31	0.55	0.19	46389	4312	28035
0.15	1.31	0.55	0.31	86289	20383	59625
0.15	1.31	0.55	0.44	105672	40304	90945
0.15	1.31	0.55	0.56	96509	42581	103590
0.15	1.31	0.55	0.69	72646	33352	86670
0.15	1.31	0.55	0.81	41321	23507	58410
0.15	1.31	0.55	0.94	19222	13068	36135
0.15	1.31	0.55	1.06	8813	7447	15570
0.15	1.31	0.65	0.06	7161	33	1845
0.15	1.31	0.65	0.19	24724	2464	10125
0.15	1.31	0.65	0.31	43267	11011	18945
0.15	1.31	0.65	0.44	49406	15279	31680
0.15	1.31	0.65	0.56	45059	16962	46035
0.15	1.31	0.65	0.69	33992	12331	42885
0.15	1.31	0.65	0.81	23058	8932	33165
0.15	1.31	0.65	0.94	11641	4785	22410
0.15	1.31	0.65	1.06	4508	2453	11745
0.15	1.87	0.35	0.06	154	11	225
0.15	1.87	0.35	0.19	1946	11	2700
0.15	1.87	0.35	0.31	3745	660	7155
0.15	1.87	0.35	0.44	5138	1969	7740
0.15	1.87	0.35	0.56	3969	2618	6660
0.15	1.87	0.35	0.69	2366	1903	3600
0.15	1.87	0.35	0.81	896	891	2205
0.15	1.87	0.35	0.94	357	451	855
0.15	1.87	0.35	1.06	91	99	135
0.15	1.87	0.45	0.06	77	11	45
0.15	1.87	0.45	0.19	931	11	630
0.15	1.87	0.45	0.31	1820	198	1440
0.15	1.87	0.45	0.44	2457	770	2250
0.15	1.87	0.45	0.56	2044	1067	2295
0.15	1.87	0.45	0.69	1323	1034	2115
0.15	1.87	0.45	0.81	798	550	1485
0.15	1.87	0.45	0.94	413	187	450
0.15	1.87	0.45	1.06	126	132	360
0.15	1.87	0.55	0.19	378	11	225
0.15	1.87	0.55	0.31	1022	66	315
0.15	1.87	0.55	0.44	1246	198	945
0.15	1.87	0.55	0.56	1134	407	630
0.15	1.87	0.55	0.69	924	253	810
0.15	1.87	0.55	0.81	616	385	990
0.15	1.87	0.55	0.94	273	176	405
0.15	1.87	0.55	1.06	154	154	405
0.15	1.87	0.65	0.19	84	11	45
0.15	1.87	0.65	0.31	140	22	135
0.15	1.87	0.65	0.44	266	77	315
0.15	1.87	0.65	0.56	168	99	315
0.15	1.87	0.65	0.69	126	77	270
0.15	1.87	0.65	0.81	140	44	450
0.15	1.87	0.65	0.94	77	11	225

Table 4: Counts in bins in Q^2 and x_B

x_B	Q^2 (GeV^2)	z	$P_\perp$ GeV	Counts π^+	π^-	π^0
0.21	1.31	0.35	0.06	73654	5060	206730
0.21	1.31	0.35	0.19	213283	83446	611865
0.21	1.31	0.35	0.31	364091	236852	857160
0.21	1.31	0.35	0.44	396788	308286	809460
0.21	1.31	0.35	0.56	268681	259468	481725
0.21	1.31	0.35	0.69	120652	141108	182340
0.21	1.31	0.35	0.81	36113	47058	41355
0.21	1.31	0.35	0.94	6090	7766	5760
0.21	1.31	0.35	1.06	497	638	630
0.21	1.31	0.45	0.06	48629	5346	82935
0.21	1.31	0.45	0.19	118762	47465	242595
0.21	1.31	0.45	0.31	193382	108944	360360
0.21	1.31	0.45	0.44	220045	153428	410400
0.21	1.31	0.45	0.56	179130	130999	332190
0.21	1.31	0.45	0.69	102354	91762	189270
0.21	1.31	0.45	0.81	43708	44759	78390
0.21	1.31	0.45	0.94	11592	12892	18810
0.21	1.31	0.45	1.06	1785	1727	2745
0.21	1.31	0.55	0.06	34783	6138	36225
0.21	1.31	0.55	0.19	76958	32208	105975
0.21	1.31	0.55	0.31	117789	58025	152055
0.21	1.31	0.55	0.44	135359	80443	189585
0.21	1.31	0.55	0.56	114149	67804	178920
0.21	1.31	0.55	0.69	76720	44649	120915
0.21	1.31	0.55	0.81	40607	27148	62280
0.21	1.31	0.55	0.94	12894	10439	21825
0.21	1.31	0.55	1.06	1841	1672	3330
0.21	1.31	0.65	0.06	27622	6666	17010
0.21	1.31	0.65	0.19	58758	24398	47295
0.21	1.31	0.65	0.31	78120	35893	69795
0.21	1.31	0.65	0.44	88690	42790	85680
0.21	1.31	0.65	0.56	75327	37279	88425
0.21	1.31	0.65	0.69	55195	22792	66150
0.21	1.31	0.65	0.81	30590	13420	39825
0.21	1.31	0.65	0.94	8687	4389	13230
0.21	1.31	0.65	1.06	889	451	1620
0.21	1.87	0.35	0.06	27727	33	54945
0.21	1.87	0.35	0.19	105763	13046	224910
0.21	1.87	0.35	0.31	198548	78694	388575
0.21	1.87	0.35	0.44	241402	140074	453330
0.21	1.87	0.35	0.56	182329	138127	364005
0.21	1.87	0.35	0.69	99771	97383	198270
0.21	1.87	0.35	0.81	39543	44385	70920
0.21	1.87	0.35	0.94	11991	13959	15570
0.21	1.87	0.35	1.06	2366	2574	3510
0.21	1.87	0.45	0.06	16765	66	16695
0.21	1.87	0.45	0.19	57449	6941	64350
0.21	1.87	0.45	0.31	99827	31878	120960
0.21	1.87	0.45	0.44	119385	57673	161910
0.21	1.87	0.45	0.56	106911	58146	153180
0.21	1.87	0.45	0.69	70343	43032	115110
0.21	1.87	0.45	0.81	35504	27148	67140
0.21	1.87	0.45	0.94	13993	12342	28305
0.21	1.87	0.45	1.06	4137	3883	10305
0.21	1.87	0.55	0.06	10864	77	4635
0.21	1.87	0.55	0.19	35721	3982	19845
0.21	1.87	0.55	0.31	58065	14410	39195
0.21	1.87	0.55	0.44	66115	25267	57915
0.21	1.87	0.55	0.56	59808	27159	63720
0.21	1.87	0.55	0.69	43505	20438	54495
0.21	1.87	0.55	0.81	25816	14366	37890
0.21	1.87	0.55	0.94	12488	7975	21780
0.21	1.87	0.55	1.06	4186	3014	10440
0.21	1.87	0.65	0.06	6622	154	1800
0.21	1.87	0.65	0.19	18221	2596	5940
0.21	1.87	0.65	0.31	27629	7447	14130
0.21	1.87	0.65	0.44	31367	10197	23625
0.21	1.87	0.65	0.56	27034	10120	29070
0.21	1.87	0.65	0.69	21476	7535	23895
0.21	1.87	0.65	0.81	14224	4763	20295
0.21	1.87	0.65	0.94	6755	2849	12375
0.21	1.87	0.65	1.06	2009	759	5490
0.27	1.31	0.35	0.06	59752	17490	183510
0.27	1.31	0.35	0.19	154693	94281	456435
0.27	1.31	0.35	0.31	224609	176242	474390
0.27	1.31	0.35	0.44	210308	177716	315720
0.27	1.31	0.35	0.56	110859	116028	120420
0.27	1.31	0.35	0.69	29225	36498	25920
0.27	1.31	0.35	0.81	2548	3663	1890
0.27	1.31	0.45	0.06	35987	15312	79290
0.27	1.31	0.45	0.19	88753	49093	218295
0.27	1.31	0.45	0.31	126987	87373	256500
0.27	1.31	0.45	0.44	136318	106007	240840
0.27	1.31	0.45	0.56	99449	80212	136620
0.27	1.31	0.45	0.69	44093	44242	56565
0.27	1.31	0.45	0.81	7798	9240	9765
0.27	1.31	0.45	0.94	196	341	405

Table 5: Counts in bins in Q^2 and x_B

x_B	Q^2 (GeV^2)	z	$P_\perp$ GeV	Counts π^+	π^-	π^0
0.27	1.31	0.55	0.06	24969	14289	40005
0.27	1.31	0.55	0.19	58604	33033	109935
0.27	1.31	0.55	0.31	79758	49137	132210
0.27	1.31	0.55	0.44	84854	60687	145710
0.27	1.31	0.55	0.56	71316	48774	107190
0.27	1.31	0.55	0.69	39487	28710	54045
0.27	1.31	0.55	0.81	8946	7557	11340
0.27	1.31	0.55	0.94	371	352	405
0.27	1.31	0.65	0.06	20951	14058	22545
0.27	1.31	0.65	0.19	46571	28567	53955
0.27	1.31	0.65	0.31	57589	32681	69300
0.27	1.31	0.65	0.44	63847	34837	74655
0.27	1.31	0.65	0.56	51975	28171	62055
0.27	1.31	0.65	0.69	28616	13827	36270
0.27	1.31	0.65	0.81	4613	2541	6075
0.27	1.31	0.65	0.94	63	44	135
0.27	1.87	0.35	0.06	56105	4081	137565
0.27	1.87	0.35	0.19	160342	59818	400995
0.27	1.87	0.35	0.31	268422	163251	587385
0.27	1.87	0.35	0.44	298116	220627	583830
0.27	1.87	0.35	0.56	209797	190179	380430
0.27	1.87	0.35	0.69	100660	112959	156285
0.27	1.87	0.35	0.81	30268	38610	42570
0.27	1.87	0.35	0.94	5474	7007	6975
0.27	1.87	0.35	1.06	315	451	675
0.27	1.87	0.45	0.06	37086	4543	54675
0.27	1.87	0.45	0.19	91504	32736	158265
0.27	1.87	0.45	0.31	143150	73227	224910
0.27	1.87	0.45	0.44	162918	104148	271980
0.27	1.87	0.45	0.56	134925	89012	232740
0.27	1.87	0.45	0.69	81599	64471	140085
0.27	1.87	0.45	0.81	35588	33176	60525
0.27	1.87	0.45	0.94	9919	9570	17595
0.27	1.87	0.45	1.06	1309	1243	2205
0.27	1.87	0.55	0.06	27188	4191	22995
0.27	1.87	0.55	0.19	59290	21131	66420
0.27	1.87	0.55	0.31	85638	37906	96435
0.27	1.87	0.55	0.44	96439	49753	121365
0.27	1.87	0.55	0.56	81144	45804	111690
0.27	1.87	0.55	0.69	56315	32131	79650
0.27	1.87	0.55	0.81	30443	19206	47520
0.27	1.87	0.55	0.94	9583	6721	15165
0.27	1.87	0.55	1.06	1519	957	2340
0.27	1.87	0.65	0.06	18515	4455	10800
0.27	1.87	0.65	0.19	41783	14531	26775
0.27	1.87	0.65	0.31	53298	21417	43380
0.27	1.87	0.65	0.44	57757	26026	50535
0.27	1.87	0.65	0.56	50050	23507	56385
0.27	1.87	0.65	0.69	35567	15466	44640
0.27	1.87	0.65	0.81	20909	8657	24930
0.27	1.87	0.65	0.94	5740	2552	7875
0.27	1.87	0.65	1.06	427	187	765
0.27	2.66	0.35	0.06	7322	22	12870
0.27	2.66	0.35	0.19	26194	2761	50625
0.27	2.66	0.35	0.31	50099	17732	92520
0.27	2.66	0.35	0.44	58891	32010	111960
0.27	2.66	0.35	0.56	45535	33055	94320
0.27	2.66	0.35	0.69	25277	22847	48420
0.27	2.66	0.35	0.81	10773	10736	18585
0.27	2.66	0.35	0.94	3164	3278	4365
0.27	2.66	0.35	1.06	476	506	360
0.27	2.66	0.45	0.06	4417	11	3285
0.27	2.66	0.45	0.19	15407	1463	13950
0.27	2.66	0.45	0.31	24773	6952	27360
0.27	2.66	0.45	0.44	29337	13167	33435
0.27	2.66	0.45	0.56	26012	13090	37350
0.27	2.66	0.45	0.69	17297	10054	27495
0.27	2.66	0.45	0.81	8372	6226	14940
0.27	2.66	0.45	0.94	3514	2893	7470
0.27	2.66	0.45	1.06	1015	858	1890

Table 6: Counts in bins in Q^2 and x_B

x_B	Q^2 (GeV^2)	z	$P_\perp$ GeV	Counts π^+	π^-	π^0
0.27	2.66	0.55	0.06	2457	11	855
0.27	2.66	0.55	0.19	8638	704	3780
0.27	2.66	0.55	0.31	13818	3553	8460
0.27	2.66	0.55	0.44	16464	5467	14310
0.27	2.66	0.55	0.56	14735	6303	14940
0.27	2.66	0.55	0.69	10941	5258	12600
0.27	2.66	0.55	0.81	6356	2860	8460
0.27	2.66	0.55	0.94	2772	1683	6300
0.27	2.66	0.55	1.06	931	671	2205
0.27	2.66	0.65	0.06	1169	11	360
0.27	2.66	0.65	0.19	3696	407	1035
0.27	2.66	0.65	0.31	5607	1419	2250
0.27	2.66	0.65	0.44	6279	1617	4410
0.27	2.66	0.65	0.56	5425	1826	6300
0.27	2.66	0.65	0.69	4200	1386	5760
0.27	2.66	0.65	0.81	2898	957	4365
0.27	2.66	0.65	0.94	1281	594	3060
0.27	2.66	0.65	1.06	280	110	855
0.33	1.31	0.35	0.06	8344	3443	26505
0.33	1.31	0.35	0.19	20636	13486	61290
0.33	1.31	0.35	0.31	27132	22286	51795
0.33	1.31	0.35	0.44	24346	19899	27990
0.33	1.31	0.35	0.56	10626	10670	9225
0.33	1.31	0.35	0.69	1617	2332	1170
0.33	1.31	0.45	0.06	4725	3091	11340
0.33	1.31	0.45	0.19	11676	7238	26145
0.33	1.31	0.45	0.31	15498	10725	31320
0.33	1.31	0.45	0.44	16730	13211	23625
0.33	1.31	0.45	0.56	10752	9350	12780
0.33	1.31	0.45	0.69	3745	3773	4140
0.33	1.31	0.45	0.81	42	66	45
0.33	1.31	0.55	0.06	3010	2519	5535
0.33	1.31	0.55	0.19	7546	4499	14805
0.33	1.31	0.55	0.31	10283	6743	18495
0.33	1.31	0.55	0.44	10619	7876	16785
0.33	1.31	0.55	0.56	8295	6061	11385
0.33	1.31	0.55	0.69	4102	2695	5130
0.33	1.31	0.55	0.81	28	22	225
0.33	1.31	0.65	0.06	2709	2563	3105
0.33	1.31	0.65	0.19	6174	4015	7020
0.33	1.31	0.65	0.31	7679	4246	9540
0.33	1.31	0.65	0.44	8176	4565	9810
0.33	1.31	0.65	0.56	6769	4070	8055
0.33	1.31	0.65	0.69	2219	1122	2790
0.33	1.87	0.35	0.06	50260	15202	138780
0.33	1.87	0.35	0.19	131222	76648	348165
0.33	1.87	0.35	0.31	191268	139150	396270
0.33	1.87	0.35	0.44	188972	151888	307440
0.33	1.87	0.35	0.56	111048	109769	144855
0.33	1.87	0.35	0.69	36183	44869	41400
0.33	1.87	0.35	0.81	5103	6358	4455
0.33	1.87	0.35	0.94	119	209	135
0.33	1.87	0.45	0.06	32067	13365	57150
0.33	1.87	0.45	0.19	76055	39886	156150
0.33	1.87	0.45	0.31	107282	66957	194445
0.33	1.87	0.45	0.44	113953	84139	200340
0.33	1.87	0.45	0.56	87675	67958	138780
0.33	1.87	0.45	0.69	44177	40744	62685
0.33	1.87	0.45	0.81	10318	11330	13635
0.33	1.87	0.45	0.94	630	759	810
0.33	1.87	0.55	0.06	21259	10890	27270
0.33	1.87	0.55	0.19	51275	27412	71505
0.33	1.87	0.55	0.31	67284	35519	92340
0.33	1.87	0.55	0.44	71631	46200	102240
0.33	1.87	0.55	0.56	58044	39853	85725
0.33	1.87	0.55	0.69	35455	24805	50760
0.33	1.87	0.55	0.81	11144	7832	15705
0.33	1.87	0.55	0.94	679	594	1485
0.33	1.87	0.65	0.06	15309	10780	14310
0.33	1.87	0.65	0.19	37597	20317	37755
0.33	1.87	0.65	0.31	45542	22561	46710
0.33	1.87	0.65	0.44	48601	24684	52785
0.33	1.87	0.65	0.56	40264	21252	46575
0.33	1.87	0.65	0.69	23177	11319	27900
0.33	1.87	0.65	0.81	5229	2552	7515
0.33	1.87	0.65	0.94	189	66	90

Table 7: Counts in bins in Q^2 and x_B

x_B	Q^2 (GeV^2)	z	$P_\perp$ GeV	Counts π^+	π^-	π^0
0.33	2.66	0.35	0.06	24325	968	50355
0.33	2.66	0.35	0.19	70203	19866	155250
0.33	2.66	0.35	0.31	116144	59565	238770
0.33	2.66	0.35	0.44	132223	88330	262305
0.33	2.66	0.35	0.56	99022	77737	195660
0.33	2.66	0.35	0.69	50813	51964	94050
0.33	2.66	0.35	0.81	16758	19569	28575
0.33	2.66	0.35	0.94	3395	4092	5670
0.33	2.66	0.35	1.06	105	132	405
0.33	2.66	0.45	0.06	15379	1111	20655
0.33	2.66	0.45	0.19	40957	10659	54675
0.33	2.66	0.45	0.31	62265	26664	83745
0.33	2.66	0.45	0.44	70497	38566	102330
0.33	2.66	0.45	0.56	59948	36278	97200
0.33	2.66	0.45	0.69	37492	26004	65250
0.33	2.66	0.45	0.81	17808	14300	34155
0.33	2.66	0.45	0.94	5243	5159	10890
0.33	2.66	0.45	1.06	504	528	1530
0.33	2.66	0.55	0.06	10591	968	7020
0.33	2.66	0.55	0.19	26117	6369	21015
0.33	2.66	0.55	0.31	37107	12540	34875
0.33	2.66	0.55	0.44	40691	17259	44415
0.33	2.66	0.55	0.56	35280	17127	41580
0.33	2.66	0.55	0.69	25011	11913	33840
0.33	2.66	0.55	0.81	13930	7744	20475
0.33	2.66	0.55	0.94	4935	2772	9945
0.33	2.66	0.55	1.06	525	352	765
0.33	2.66	0.65	0.06	6447	902	3105
0.33	2.66	0.65	0.19	16079	3773	8505
0.33	2.66	0.65	0.31	20692	6787	14355
0.33	2.66	0.65	0.44	22337	7843	17100
0.33	2.66	0.65	0.56	19397	6941	20610
0.33	2.66	0.65	0.69	14231	6039	16920
0.33	2.66	0.65	0.81	8113	3267	10800
0.33	2.66	0.65	0.94	2562	737	4500
0.33	2.66	0.65	1.06	84	44	270
0.33	3.79	0.35	0.19	245	11	450
0.33	3.79	0.35	0.31	392	132	765
0.33	3.79	0.35	0.44	602	330	990
0.33	3.79	0.35	0.56	455	187	900
0.33	3.79	0.35	0.69	217	121	270
0.33	3.79	0.35	0.81	105	143	180
0.33	3.79	0.35	0.94	56	88	135
0.33	3.79	0.45	0.19	98	11	45
0.33	3.79	0.45	0.31	224	66	360
0.33	3.79	0.45	0.44	210	66	270
0.33	3.79	0.45	0.56	210	132	360
0.33	3.79	0.45	0.69	133	99	90
0.33	3.79	0.45	0.81	63	44	270
0.33	3.79	0.55	0.31	98	22	180
0.33	3.79	0.55	0.44	133	22	90
0.33	3.79	0.55	0.56	126	22	135
0.33	3.79	0.55	0.69	98	55	90
0.33	3.79	0.55	0.81	91	22	135
0.39	1.87	0.35	0.06	15106	6655	39375
0.39	1.87	0.35	0.19	36400	21670	92745
0.39	1.87	0.35	0.31	49840	37224	97335
0.39	1.87	0.35	0.44	46487	39490	64980
0.39	1.87	0.35	0.56	24493	24816	27315
0.39	1.87	0.35	0.69	5614	6468	5265
0.39	1.87	0.35	0.81	77	88	45
0.39	1.87	0.45	0.06	9457	4994	17010
0.39	1.87	0.45	0.19	20972	11616	44235
0.39	1.87	0.45	0.31	28119	18326	52065
0.39	1.87	0.45	0.44	29330	23122	50400
0.39	1.87	0.45	0.56	22764	18370	31950
0.39	1.87	0.45	0.69	9373	8415	11430
0.39	1.87	0.45	0.81	518	583	585

Table 8: Counts in bins in Q^2 and x_B

x_B	Q^2 (GeV^2)	z	$P_\perp$ GeV	Counts π^+	π^-	π^0
0.39	1.87	0.55	0.06	5845	4345	7470
0.39	1.87	0.55	0.19	13384	8415	22590
0.39	1.87	0.55	0.31	18270	10098	25965
0.39	1.87	0.55	0.44	18683	12705	27540
0.39	1.87	0.55	0.56	16422	11352	21870
0.39	1.87	0.55	0.69	8190	5918	10260
0.39	1.87	0.55	0.81	518	341	720
0.39	1.87	0.65	0.06	4242	3685	4995
0.39	1.87	0.65	0.19	10780	6413	11790
0.39	1.87	0.65	0.31	13524	6314	12915
0.39	1.87	0.65	0.44	13720	7260	15660
0.39	1.87	0.65	0.56	11417	6413	13320
0.39	1.87	0.65	0.69	4004	2387	5625
0.39	1.87	0.65	0.81	70	44	135
0.39	2.66	0.35	0.06	28406	6149	72630
0.39	2.66	0.35	0.19	75460	35145	187065
0.39	2.66	0.35	0.31	112693	74448	238770
0.39	2.66	0.35	0.44	116564	86306	226035
0.39	2.66	0.35	0.56	80430	71467	140400
0.39	2.66	0.35	0.69	33845	37631	49185
0.39	2.66	0.35	0.81	6951	8701	10755
0.39	2.66	0.35	0.94	350	572	630
0.39	2.66	0.45	0.06	18235	5005	28845
0.39	2.66	0.45	0.19	43463	19426	76500
0.39	2.66	0.45	0.31	64190	33968	100170
0.39	2.66	0.45	0.44	67886	44319	115650
0.39	2.66	0.45	0.56	52948	38863	91620
0.39	2.66	0.45	0.69	31430	25124	51120
0.39	2.66	0.45	0.81	9583	9713	17145
0.39	2.66	0.45	0.94	1127	1067	2250
0.39	2.66	0.55	0.06	12761	4092	13005
0.39	2.66	0.55	0.19	30667	11693	33390
0.39	2.66	0.55	0.31	39172	17182	43920
0.39	2.66	0.55	0.44	41979	21681	51795
0.39	2.66	0.55	0.56	35000	20141	50805
0.39	2.66	0.55	0.69	21623	12848	30195
0.39	2.66	0.55	0.81	8589	5313	13590
0.39	2.66	0.55	0.94	1120	726	1935
0.39	2.66	0.65	0.06	8316	3597	6210
0.39	2.66	0.65	0.19	21063	8338	15165
0.39	2.66	0.65	0.31	25424	10439	19215
0.39	2.66	0.65	0.44	27153	11110	23760
0.39	2.66	0.65	0.56	24143	9823	24120
0.39	2.66	0.65	0.69	14588	6688	15840
0.39	2.66	0.65	0.81	4368	1815	5130
0.39	2.66	0.65	0.94	252	66	450
0.39	3.79	0.35	0.06	3150	11	5760
0.39	3.79	0.35	0.19	10318	1694	19800
0.39	3.79	0.35	0.31	18095	6952	30735
0.39	3.79	0.35	0.44	19950	11528	37755
0.39	3.79	0.35	0.56	14658	10186	30645
0.39	3.79	0.35	0.69	7469	6864	16605
0.39	3.79	0.35	0.81	2772	3124	5625
0.39	3.79	0.35	0.94	469	539	990
0.39	3.79	0.45	0.06	1771	22	1395
0.39	3.79	0.45	0.19	5901	748	5670
0.39	3.79	0.45	0.31	9163	2431	10440
0.39	3.79	0.45	0.44	10549	4895	12825
0.39	3.79	0.45	0.56	9079	4499	12870
0.39	3.79	0.45	0.69	5334	3014	8775
0.39	3.79	0.45	0.81	2814	2013	5085
0.39	3.79	0.45	0.94	644	649	1440
0.39	3.79	0.55	0.06	1589	11	495
0.39	3.79	0.55	0.19	3339	583	1665
0.39	3.79	0.55	0.31	5376	1474	3645
0.39	3.79	0.55	0.44	5649	1639	5445
0.39	3.79	0.55	0.56	5159	2167	4365
0.39	3.79	0.55	0.69	3458	1562	4500
0.39	3.79	0.55	0.81	1883	1023	3240
0.39	3.79	0.55	0.94	672	275	1170

Table 9: Counts in bins in Q^2 and x_B

x_B	Q^2 (GeV^2)	z	$P_\perp$ GeV	Counts π^+	π^-	π^0
0.39	3.79	0.65	0.06	658	22	315
0.39	3.79	0.65	0.19	1687	209	540
0.39	3.79	0.65	0.31	2191	561	1665
0.39	3.79	0.65	0.44	2562	649	1800
0.39	3.79	0.65	0.56	2107	638	2115
0.39	3.79	0.65	0.69	1666	638	1980
0.39	3.79	0.65	0.81	896	286	990
0.39	3.79	0.65	0.94	196	77	540
0.45	2.66	0.35	0.06	14357	5423	36990
0.45	2.66	0.35	0.19	37555	21043	91080
0.45	2.66	0.35	0.31	49658	36696	103230
0.45	2.66	0.35	0.44	48559	39710	91170
0.45	2.66	0.35	0.56	32200	29898	46080
0.45	2.66	0.35	0.69	9751	11396	12600
0.45	2.66	0.35	0.81	546	693	405
0.45	2.66	0.45	0.06	8113	4081	16200
0.45	2.66	0.45	0.19	21161	11022	40320
0.45	2.66	0.45	0.31	29386	17017	53775
0.45	2.66	0.45	0.44	30331	21901	53100
0.45	2.66	0.45	0.56	23709	18601	40995
0.45	2.66	0.45	0.69	12033	10076	18360
0.45	2.66	0.45	0.81	1652	1441	2025
0.45	2.66	0.55	0.06	5439	3102	7920
0.45	2.66	0.55	0.19	15274	7645	18090
0.45	2.66	0.55	0.31	18564	9262	21915
0.45	2.66	0.55	0.44	19320	10802	23715
0.45	2.66	0.55	0.56	16044	10186	22725
0.45	2.66	0.55	0.69	8820	5951	13455
0.45	2.66	0.55	0.81	1057	946	1935
0.45	2.66	0.65	0.06	3822	2717	2925
0.45	2.66	0.65	0.19	10983	5049	9180
0.45	2.66	0.65	0.31	12943	5621	11790
0.45	2.66	0.65	0.44	13419	6523	12510
0.45	2.66	0.65	0.56	11221	5797	11970
0.45	2.66	0.65	0.69	4606	1859	5805
0.45	2.66	0.65	0.81	280	77	315
0.45	3.79	0.35	0.06	7217	407	16515
0.45	3.79	0.35	0.19	19621	7073	45540
0.45	3.79	0.35	0.31	30786	17204	62505
0.45	3.79	0.35	0.44	32347	22924	66555
0.45	3.79	0.35	0.56	23856	19536	46800
0.45	3.79	0.35	0.69	11725	11341	21465
0.45	3.79	0.35	0.81	2765	3333	5220
0.45	3.79	0.35	0.94	77	121	225
0.45	3.79	0.45	0.06	4865	550	6570
0.45	3.79	0.45	0.19	11578	3509	16065
0.45	3.79	0.45	0.31	17346	7513	24435
0.45	3.79	0.45	0.44	18627	10615	27090
0.45	3.79	0.45	0.56	15407	9702	24390
0.45	3.79	0.45	0.69	8967	6765	17505
0.45	3.79	0.45	0.81	3045	2926	6750
0.45	3.79	0.45	0.94	280	264	405
0.45	3.79	0.55	0.06	3437	374	2295
0.45	3.79	0.55	0.19	8316	2321	5625
0.45	3.79	0.55	0.31	10563	3597	9450
0.45	3.79	0.55	0.44	10920	4675	11295
0.45	3.79	0.55	0.56	9079	4807	10575
0.45	3.79	0.55	0.69	6153	3168	9270
0.45	3.79	0.55	0.81	2625	1408	4500
0.45	3.79	0.55	0.94	245	99	675
0.45	3.79	0.65	0.06	2121	407	630
0.45	3.79	0.65	0.19	5257	1408	2655
0.45	3.79	0.65	0.31	5817	1870	4365
0.45	3.79	0.65	0.44	6650	2156	5220
0.45	3.79	0.65	0.56	5852	1958	4770
0.45	3.79	0.65	0.69	4074	1639	4230
0.45	3.79	0.65	0.81	1288	539	1485